OXFORD

Human Molecular Genetics, 2018, Vol. 27, No. 5 837–852

doi: 10.1093/hmg/ddy004
Advance Access Publication Date: 3 January 2018
Original Article

ORIGINAL ARTICLE

Cytosolic HSC20 integrates *de novo* iron–sulfur cluster biogenesis with the CIAO1-mediated transfer to recipients

Ki Soon Kim†, Nunziata Maio†, Anamika Singh and Tracey A. Rouault*

Molecular Medicine Branch, Eunice Kennedy Shriver National Institute of Child Health and Human Development, Bethesda, MD 20892, USA

*To whom correspondence should be addressed at: Section on Human Iron Metabolism, Eunice Kennedy Shriver National Institute of Child Health and Human Development, National Institutes of Health, Bldg 35A, Rm 2D824, Bethesda, MD 20892, USA. Tel: +1 3014967060; Fax: +1 3014969939; Email: rouault@mail.nih.gov

Abstract

Iron–sulfur (Fe-S) clusters are cofactors in hundreds of proteins involved in multiple cellular processes, including mitochondrial respiration, the maintenance of genome stability, ribosome biogenesis and translation. Fe-S cluster biogenesis is performed by multiple enzymes that are highly conserved throughout evolution, and mutations in numerous biogenesis factors are now recognized to cause a wide range of previously uncategorized rare human diseases. Recently, a complex formed of components of the cytoplasmic Fe-S cluster assembly (CIA) machinery, consisting of CIAO1, FAM96B and MMS19, was found to deliver Fe-S clusters to a subset of proteins involved in DNA metabolism, but it was unclear how this complex acquired its fully synthesized Fe-S clusters, because Fe-S clusters have been alleged to be assembled *de novo* solely in the mitochondrial matrix. Here, we investigated the potential role of the human cochaperone HSC20 in cytosolic Fe-S assembly and found that HSC20 assists Fe-S cluster delivery to cytosolic and nuclear Fe-S proteins. Cytosolic HSC20 (C-HSC20) mediated complex formation between components of the cytosolic Fe-S biogenesis pathway (ISC), including the primary scaffold, ISCU1, and the cysteine desulfurase, NFS1, and the CIA targeting complex, consisting of CIAO1, FAM96B and MMS19, to facilitate Fe-S cluster insertion into cytoplasmic and nuclear Fe-S recipients. Thus, C-HSC20 integrates initial Fe-S biosynthesis with the transfer activities of the CIA targeting system. Our studies demonstrate that a novel cytosolic pathway functions in parallel to the mitochondrial ISC to perform *de novo* Fe-S biogenesis, and to escort Fe-S clusters to cytoplasmic and nuclear proteins.

Introduction

In addition to their known importance in mitochondrial respiration, iron–sulfur (Fe-S) clusters are irreplaceable cofactors in several DNA processing enzymes, including the DNA helicase XPD and its associated family members that act in DNA replication and repair (1–5). Among the emerging roles of Fe-S clusters in maintaining genome stability is their proposed ability to function as redox sensors, which enables Fe-S repair enzymes to probe DNA integrity and localize sites of DNA damage through electron transfer reactions, and to regulate the binding of DNA primases and polymerases (6,7).

Biogenesis of all Fe-S proteins depends on the core Fe-S cluster (ISC) assembly machinery (8,9). Additionally, multiple eukaryotic cytosolic and nuclear Fe-S enzymes require the function of proteins unique to the cytoplasmic Fe-S cluster assembly (CIA) machinery for cluster acquisition. In mammalian cells, Fe-S clusters are assembled by a complex composed of a cysteine desulfurase, NFS1, its binding partner, ISD11 (also known as LYRM4), the acyl carrier protein (ACP), the ISCU scaffold, and an

†These authors contributed equally to this work.
Received: October 30, 2017. **Revised:** December 5, 2017. **Accepted:** December 29, 2017

iron donor or allosteric effector, frataxin (9–11). Upon assembly of a nascent (Fe_2-S_2) cluster, the scaffold protein ISCU binds to a highly conserved J-protein (also known as cochaperone), known as HscB in bacteria, Jac1 in yeast and HSC20 in human, and to an HSP70 chaperone, known as HscA in bacteria, Ssq1 in yeast and HSPA9 in human (12–15). The ATP-driven conformational change of the HSP70, activated by the cochaperone, enhances transfer of the ISCU-bound cluster to recipient apoproteins or to secondary scaffolds that then deliver the cluster to specific subsets of final acceptors (13).

In *Saccharomyces cerevisiae*, the cysteine desulfurase Nfs1 is present in mitochondria (16) and in the nucleus (17), whereas other ISC components have previously been detected exclusively in mitochondria (18,19), leading to the proposal that *de novo* Fe-S cluster assembly occurs only in the mitochondrial compartment, whereas assembly of extra-mitochondrial Fe-S cofactors requires export of a sulfur-containing compound from the mitochondrial matrix to the cytosol (8,16). Importantly, the core mammalian ISC components have been previously identified not only in the mitochondrial matrix, but also in the cytosol and nucleus (14,15,20–25), suggesting that Fe-S cluster biogenesis machineries may independently operate in parallel to generate nascent Fe-S clusters in the subcellular compartments of multicellular eukaryotes. Cytosolic NFS1 (C-NFS1) is an active cysteine desulfurase, which is integral to the process of sulfur mobilization for molybdenum cofactor (MoCo) biosynthesis and tRNA thiolation (17,26–29). C-NFS1 was also previously found to form a complex with the cytosolic isoform of the main scaffold protein, ISCU1. Cytosolic ISCU (named ISCU1) is an alternative isoform generated by the same *ISCU* gene that encodes mitochondrial ISCU (named ISCU2). ISCU1 lacks the mitochondrial targeting sequence and localizes to the cytosol (30).

HSC20 is the sole human cochaperone dedicated to Fe-S cluster biogenesis (14). Mutations in HSC20 and in its orthologs cause defects in Fe-S protein activities, mitochondrial iron accumulation, and reduced mitochondrial respiration in human cell lines (14,31), and in multiple experimental systems, including yeast (32,33) and fly (34). The importance of Fe-S biogenesis for human health is well established, as mutations that affect proteins involved in the pathway cause several distinctive human diseases (9,35). HSC20 is an essential Fe-S biogenesis factor that has also been detected in the cytosol of mammalian and plant cells (14,15,36). In mitochondria, HSC20 directly binds consensus sequences known as LYR (Leucine-Tyrosine-Arginine) motifs to assist biogenesis of the respiratory chain complexes I–III (15,31).

Biogenesis of cytosolic and nuclear Fe-S proteins depends on the coordination of the ISC and CIA biogenesis machineries. In 2012, two independent studies demonstrated that the highly conserved HEAT repeat protein MMS19, in complex with CIAO1 (also known as WDR39 or Cia1 yeast) and FAM96B (also known as MIP18), was required for Fe-S transfer to enzymes involved in DNA metabolism (37,38). However, the mechanism by which the CIA complex acquires and facilitates transfer of Fe-S clusters has remained unclear. Elucidating the pathway that underlies biogenesis of cytosolic and nuclear Fe-S enzymes may illuminate mechanisms of diseases associated with genome instability (39–41), in addition to providing insights into fundamental aspects of Fe-S protein assembly.

In the present study, we investigated the potential role of the cochaperone HSC20 in the biogenesis of Fe-S clusters in the cytosolic compartment of mammalian cells. Using a combination of proteomic and functional approaches, we found that cytosolic HSC20 (C-HSC20) promotes activity of a *de novo* Fe-S biogenesis pathway (ISC) that functions in parallel to the well-described mitochondrial pathway. C-HSC20 mediated complex formation between the ISC and the CIA machineries by directly binding to the scaffold protein ISCU1 of the ISC system and to CIAO1 of the CIA targeting complex, to bridge the nascent ISC pathway with the CIA Fe-S transfer platform built around CIAO1. Here, we have demonstrated that formation of a large ISC/CIA multi-protein complex is required for Fe-S cluster insertion in multiple proteins involved in DNA metabolism, ribosome biogenesis and translation. In the absence of HSC20 or upon expression of a dominant negative mutant of the cytosolic isoform of the main scaffold ISCU1, failure to transfer Fe-S clusters to target cytosolic and nuclear proteins resulted in loss of activity and stability of Fe-S enzymes. Our studies establish that C-HSC20 is indispensable for cytoplasmic Fe-S assembly and delivery, which is initiated *de novo* in the cytosol.

Results

The crosstalk between the cytosolic ISC and CIA machineries occurs through the physical interaction of their core components, which is mediated by C-HSC20

To identify interacting partners of C-HSC20 and gain insights into the function of the cochaperone in the cytosol of mammalian cells, we performed mass spectrometry (MS) analysis on the eluates after immunoprecipitation (IP) of endogenous HSC20 from cytosolic fractions isolated from HEK293 cells. Only proteins that specifically co-purified with HSC20 in the IP with anti-rabbit HSC20 antibody and not in the negative control (anti-rabbit IgG) were considered for further analysis and are listed in Supplementary Material, Figure S1A. C-HSC20 corresponded to the full-length protein (residues 1–235 of HSC20), as several peptides identified by MS covered the N-terminal sequence of the cochaperone (Supplementary Material, Fig. S1A), which has previously been designated as a mitochondrial targeting sequence that is cleaved upon mitochondrial uptake. Our findings are consistent with the increased MW of C-HSC20 compared to the mature processed mitochondrial HSC20 (Fig. 1A, top panel), and demonstrate that C-HSC20 is a distinct isoform of the cytosolic compartment (Fig. 1A and Supplementary Material, Fig. S1A and B). Among the interacting partners of C-HSC20 identified by MS were core components of the ISC machinery, consisting of the chaperone HSPA9 and the scaffold ISCU, along with several known CIA proteins, including CIAO1, MMS19 and FAM96B, the P-loop NTPase NUBP2, GLRX3 and BOLA2, which are thought to function as Fe-S intermediate carriers (42), and CIAPIN1, which is proposed to be part of the electron transfer chain of the CIA system (43). Moreover, several recipient Fe-S proteins were identified as HSC20 interacting partners, such as ABCE1, which plays a crucial role in ribosome biogenesis and translation, PPAT, involved in purine biosynthesis, and several enzymes involved in DNA metabolism (ERCC2, DDX11, POLD1, POLE, PRIM2, CDKAL1, ELP3, CPSF30) (Supplementary Material, Fig. S1A). We validated multiple putative interacting partners of C-HSC20 by co-immunoprecipitation (co-IP). Reciprocal co-IP experiments confirmed that C-HSC20 interacted with the components of the targeting complex, CIAO1, MMS19, FAM96B, and with the recipient Fe-S proteins POLD1 and ELP3 (Fig. 1A). To further analyze the network of interactions revealed by the MS analysis and characterize distinct molecular complexes containing C-HSC20 and its interacting partners, we immunoprecipitated FLAG-tagged

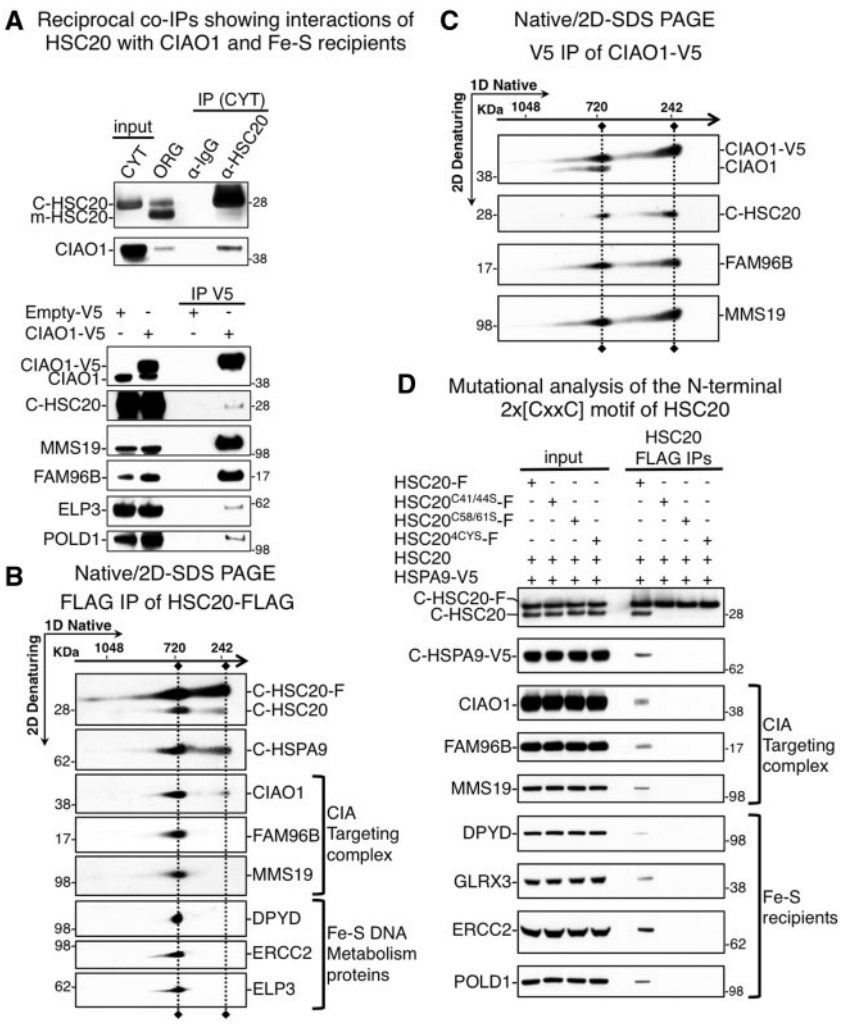

Figure 1. C-HSC20 interacts with core components of the ISC and CIA machineries during biogenesis of cytosolic and nuclear Fe-S proteins. (**A**) Upper panel, IP of endogenous HSC20 from cytosolic fractions (CYT), followed by immunoblot (IB) to CIAO1 (C-HSC20). Organellar fractions (ORG) were loaded on the gel for comparison. Lower panel, IP of stably expressed CIAO1-V5 from cytosolic fractions, followed by IBs to CIAO1, HSC20, MMS19, FAM96B and the Fe-S proteins ELP3 and POLD1. (**B**) Anti-FLAG IP of HSC20-FLAG from cytosolic fractions. Native/2D-SDS-PAGE analysis was performed on the competitively eluted complexes, followed by IBs to HSC20, HSPA9, CIAO1, FAM96B, MMS19, and the Fe-S proteins DPYD, ERCC2 and ELP3. (**C**) IP of CIAO-V5 was performed on cytosolic fractions from cells stably expressing CIAO1-V5. Competitively eluted complexes were subjected to native followed by 2D-SDS-PAGE analysis. IBs to CIAO1, HSC20, FAM96B and MMS19 were performed to identify components of multimeric complexes. (**D**) Cytosolic fractions from cells stably expressing HSPA9-V5 and transiently cotransfected with HSC20 (without a C-terminal FLAG tag) and either with FLAG-tagged HSC20 wild-type (WT), or the mutants of the N-terminal cysteine residues, as indicated, were subjected to anti-FLAG IPs. Eluates were analyzed for the presence of HSC20, HSPA9, CIAO1, FAM96B, MMS19, and the Fe-S proteins DPYD, GLRX3, ERCC2, and POLD1 (A–D, $n = 5$ biological replicates). See also Supplementary Material, Figure S1.

C-HSC20 and performed two-dimensional gel electrophoresis (2D denaturing PAGE), after resolving individual multimeric cytosolic complexes by native PAGE (1D Native). We demonstrated that C-HSC20 interacted with its cognate chaperone HSPA9, with the CIA complex formed of CIAO1, FAM96B and MMS19, and with the Fe-S proteins dihydropyrimidine dehydrogenase (DPYD), ERCC2 and ELP3 (Fig. 1B), as shown by the colocalization of these proteins in the same immunopurified complexes containing C-HSC20. Reciprocal co-IP of V5-tagged CIAO1 further confirmed the interaction with C-HSC20 (Fig. 1C). Notably, endogenous CIAO1 coimmunoprecipitated with CIAO1-V5 in the complex close to the 720 kDa marker (Fig. 1C), indicating that more than one CIAO1 molecule was present in this large multimeric complex.

Mutagenesis of a zinc-finger like dimerization motif at the N terminus of C-HSC20 abrogated binding to the Fe-S biogenesis complexes and to Fe-S recipients

We previously reported that HSC20 has the ability to dimerize in the mitochondrial compartment of mammalian cells (15). We found that FLAG-tagged C-HSC20 co-immunoprecipitated endogenous C-HSC20 (Fig. 1B, complexes at 242 and 720 kDa) and we sought to further investigate the physiological relevance of the dimerization of C-HSC20. The human cochaperone has two unique Cys-xx-Cys modules (consisting of Cys41, Cys44, Cys58 and Cys61), which coordinate zinc at the N terminus (44). Zinc-binding domains are known to mediate dimerization of several proteins (45). Upon mutagenizing residues of the

zinc-binding domain of HSC20, we found that substitution of a pair of cysteines with serines in the two CxxC modules (in $HSC20^{C41/44S}$ or $HSC20^{C58/61S}$) or mutagenesis of all four cysteines into serines in $HSC20^{4CYS}$ abolished the dimerization of HSC20 (Fig. 1D, top panel) and concomitantly disrupted its interactions with its cognate chaperone HSPA9, identified in our MS analysis, and also with the CIA complex, as well as with the Fe-S recipients DPYD, GLRX3, ERCC2 and POLD1 (Fig. 1D), indicating that dimerization of C-HSC20 is crucial for establishing the network of interactions that we have reported here.

De novo Fe-S cluster assembly occurred in the cytosol of mammalian cells

One of the most relevant and controversial questions on Fe-S cluster biogenesis in the cytosol of mammalian cells pertains to the identity of the main scaffold protein upon which the cluster is assembled. In our MS data, we found that C-HSC20 interacted with ISCU1, the cytosolic isoform of the main scaffold upon which the cluster is initially assembled. In most model systems, *de novo* assembly of the cluster on ISCU requires that the cysteine desulfurase NFS1 interact directly with the primary scaffold. A cytosolic isoform of the cysteine desulfurase NFS1 (C-NFS1), previously identified in mammalian cells (20), was found to be generated by initiation of translation at the second in-frame AUG of the *NFS1* transcript. C-NFS1 lacks the first 60 amino acid residues of the mitochondrial precursor form, and resides in both the cytosol and nucleus (20). Therefore, we characterized interactions of C-NFS1 by performing IP of endogenous C-NFS1 on cytosolic fractions from HEK293 cells. Several C-NFS1 binding partners were identified in eluates using MS (Supplementary Material, Fig. S2A).

C-NFS1 binds to components of the ISC and CIA machineries in multimeric cytosolic complexes

We found that C-NFS1 interacted with the main scaffold ISCU, with C-HSC20, with HSPA9, CIAO1, FAM96B, and with several Fe-S proteins, including ELP3, GLRX3, BOLA2, ABCE1, PRIM2, PPAT, POLD1 and DDX11 in three independent IP experiments followed by MS analyses (Supplementary Material, Fig. S2A). Interestingly, the fatty acid synthase FASN was a C-NFS1 interacting partner (Supplementary Material, Fig. S2A and B). Co-IP experiments confirmed that FASN interacted with endogenous C-NFS1 (Supplementary Material, Fig. S2C), as well as with FLAG-tagged C-NFS1 (C-NFS1-F) (Supplementary Material, Fig. S2D). Mammalian FASN is a single, multifunctional polypeptide, which contains an ACP domain (46). The interaction of C-NFS1 with FASN is intriguing, as the ACP has been recently characterized as an integral component of the active cysteine desulfurase complex in mitochondria (11,47–49). We also identified the adenylyl- and sulfur-transferase MOCS3 and the Ubiquitin-related modifier 1 (URM1), as C-NFS1 interacting partners by MS (Supplementary Material, Fig. S2A), and we validated these interactions by co-IP (Supplementary Material, Fig. S2D). MOCS3 is involved in MoCo biosynthesis, and URM1 in tRNA thiolation. Our results are consistent with previous studies that described a novel role of C-NFS1 as a sulfur donor enzyme for MoCo biosynthesis and tRNA thiolation (26,50), and reveal that a physical interaction between C-NFS1 and MOCS3 or URM1 is required for these essential biological pathways. ISD11, a protein critical for the function of the cysteine desulfurase complex in eukaryotes, was not identified in our MS data as an interacting partner of C-NFS1 at the false discovery rate (FDR) of 1% set in our analyses. However, when the FDR was increased to 2%, ISD11 was present in all three independent IPs of C-NFS1 analyzed by MS, but not in the negative controls (anti-mouse IgG), consistent with previous studies that demonstrated the interaction between C-NFS1 and ISD11 (21,26).

To confirm the protein interaction data obtained by MS and assess activities of the Fe-S cluster biogenesis machinery in the cytosol, we generated two stable cell lines that expressed either wild-type cytosolic ISCU1, or a dominant negative mutant that is expected to interfere with Fe-S assembly, $ISCU1^{D46A}$, under the control of a doxycycline-inducible promoter. Asp46 of human cytosolic ISCU1 corresponds to Asp71 of the mitochondrial isoform ISCU2. Substitution of this highly conserved Asp residue into Ala in bacteria was found to impair transfer of nascent Fe-S clusters from IscU to downstream recipients (51–53). Upon induction of expression of the $ISCU1^{D46A}$ mutant for 24 or 48 h, we detected a significant reduction in the levels of POLD1, ELP3 and ERCC2 proteins (Fig. 2A and Supplementary Material, Fig. S2E), which is consistent with previous observations that Fe-S apoproteins often undergo degradation when they fail to acquire their Fe-S prosthetic groups (15,54,55).

We tested the ability of ISCU1 to interact with components of the Fe-S biogenesis machinery by performing IPs of wild-type ISCU1 or the D46A mutant expressed for 16 h, and analyzing the eluates either by traditional Sodium dodecyl sulphate-polyacrylamide gel electrophoresis (SDS-PAGE) and immunoblot (Fig. 2B), or by native PAGE followed by 2D-SDS-PAGE (Fig. 2C). We found that wild-type ISCU1 interacted with endogenous C-NFS1 and with C-HSC20, with the components of the CIA targeting complex, and with Fe-S recipients (Fig. 2B and C); conversely, $ISCU1^{D46A}$-MYC interacted strongly with C-NFS1, but binding to HSC20, CIAO1, MMS19, POLD1 and ERCC2 was almost undetectable (Fig. 2B and E). ^{55}Fe-radiolabeling of cells expressing ISCU1 wild-type or the D46A mutant showed that $ISCU1^{D46A}$ retained high amounts of radiolabeled iron, whereas wild-type ISCU1-MYC did not (Fig. 2E). ^{55}Fe incorporation into POLD1 decreased significantly in cells that expressed $ISCU1^{D46A}$ (Fig. 2F). Our data are consistent with previous studies on the mutated orthologs of ISCU, which similarly showed stabilization of the cluster on ISCU and impaired transfer to Fe-S recipients (51–53). Overall, these results demonstrated that ISCU1 was able to ligate a cluster, and function as a cytosolic scaffold protein, from which the cluster was subsequently transferred to recipient Fe-S proteins by the HSC20/HSPA9 complex.

C-HSC20 mediated formation of a large ISC/CIA multiprotein complex, which contained core components of the two machineries, along with Fe-S recipients

In our MS analysis, C-HSC20 appeared to play a central role in cytosolic Fe-S biogenesis, as it was found to bind components of the ISC and CIA machineries, as well as several Fe-S recipients (Supplementary Material, Fig. S1A). To further investigate the role of C-HSC20 in cytosolic Fe-S cluster biogenesis, we knocked out its expression by CRISPR/Cas9 (Supplementary Material, Fig. S3A and B), and analyzed the cytosolic fractions by SDS-PAGE, native immunoblots or a combination of native and 2D-SDS-PAGE. C-HSC20 was efficiently knocked out, leading to undetectable protein levels on cytosolic fractions from the single knock out (KO) cell clone used in our studies (Supplementary Material, Fig. S3C). Levels of components of the

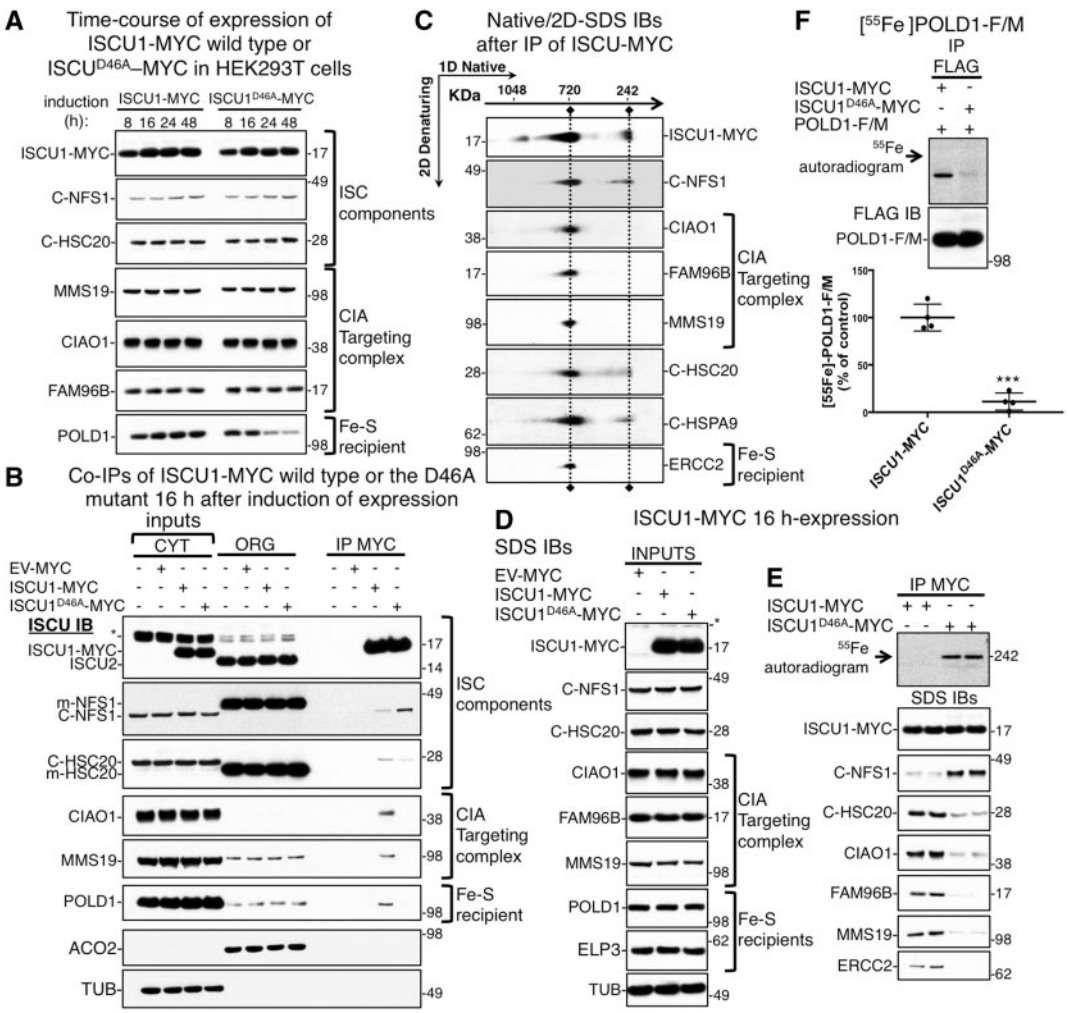

Figure 2. Expression of a dominant negative mutant of the cytosolic scaffold protein ISCU, ISCU1^{D46A}, impairs cytoplasmic Fe-S cluster biogenesis. (**A**) Time-course of expression of inducible ISCU1-MYC WT or the D46A mutant. Cytosolic fractions were analyzed at the indicated time points by western blot to assess levels of ISCU1-MYC recombinant proteins, MMS19, CIAO1, FAM96B, C-NFS1, C-HSC20 and POLD1. (**B**) IPs of ISCU1-MYC WT or the D46A mutant on cytosolic fractions (CYT). Samples were subjected to IBs to ISCU, NFS1, HSC20, CIAO1, MMS19 and POLD1. The asterisk indicates a nonspecific band (ORG corresponds to organellar fractions, which were loaded on the gel for comparison with the cytosolic extracts). IBs to mitochondrial aconitase (ACO2) and tubulin (TUB) were included as controls for the subcellular fractionation. (**C**) IP of ISCU1-MYC from cytosolic fractions. Native and 2D-SDS PAGE analysis were followed by IBs to MYC tag, NFS1, CIAO1, FAM96B, MMS19, HSC20, HSPA9 and ERCC2. (**D**) Cytosolic fractions from control cells (EV-MYC, which corresponds to cells stably transfected with the empty vector, as a negative control) and from cells expressing ISCU1-MYC WT or the D46A mutant for 16 h were used as inputs to immunoprecipitate ISCU1-MYC (IP samples are shown in E). (**E**) Anti-MYC IPs of ISCU1-MYC WT or the D46A mutant from cells labeled for 5 days with ^{55}Fe-transferrin. Eluates after anti-MYC IPs of WT or mutant ISCU1 were analyzed by ^{55}Fe autoradiogram (top), or by IBs to MYC, NFS1, HSC20, CIAO1, FAM96B, MMS19, and ERCC2 to search for interacting partners of ISCU1 (lower panels). (**F**) ^{55}Fe incorporation into POLD1-FLAG/MYC transiently transfected in cells stably expressing ISCU1-MYC WT or the D46A mutant for 16 h, and anti-FLAG IB to verify that equal amounts of POLD1-F/M were immunoprecipitated. Lower panel, quantification of radioactive iron incorporated into POLD1-F/M shown in the autoradiogram. [^{55}Fe]-POLD1-F/M and POLD1-F/M were quantified and the ratio was normalized to control (cells expressing ISCU1-MYC), set to 100%. Values are expressed as % of control and are given as mean ± SEM. $P < 0.001$ (A–F, $n = 4$ biological replicates). See also Supplementary Material, Figure S2.

CIA targeting complex, CIAO1, FAM96B, MMS19 did not change upon CRISPR of HSC20 (Supplementary Material, Fig. S3C). We observed loss of several Fe-S proteins, including POLD1, ELP3, DPYD and PPAT in the absence of HSC20 (Supplementary Material, Fig. S3C). Native IBs on cytosolic fractions from control or *C-HSC20*-KO cells revealed that the CIA targeting complex was able to assemble even in the absence of HSC20, though to a lesser extent compared with control cells (Fig. 3B, complex labeled CIA at 240 kDa). The C-NFS1/ISCU1 interaction was stabilized in the *C-HSC20* KO cell clone (Fig. 3A, complex labeled C-ISC), consistent with the notion that the cochaperone–chaperone system facilitates release of the nascent cluster from ISCU1 for transfer to recipient proteins, and that the cluster that was initially synthesized remained trapped on ISCU1 in the absence of HSC20.

A cytosolic complex of apparent MW of 720 kDa contained the cytosolic ISC core proteins (C-ISC), ISCU1, NFS1, HSC20 (Fig. 3A, complex labeled C-ISC/CIA), the CIA targeting components, CIAO1, FAM96B, MMS19 (Fig. 3B, complex labeled C-ISC/CIA), along with recipient Fe-S proteins, including POLD1, ELP3, DPYD (Fig. 3C, complex labeled C-ISC/CIA). Interestingly, the C-ISC/CIA complex failed to assemble upon KO of *HSC20* (Fig. 3A–C), indicating that C-HSC20 was required to merge the CIA and the cytosolic ISC components into a single complex of ~720 kDa during cytosolic Fe-S cluster biogenesis. Resolution of the native cytosolic complexes in the second dimension by

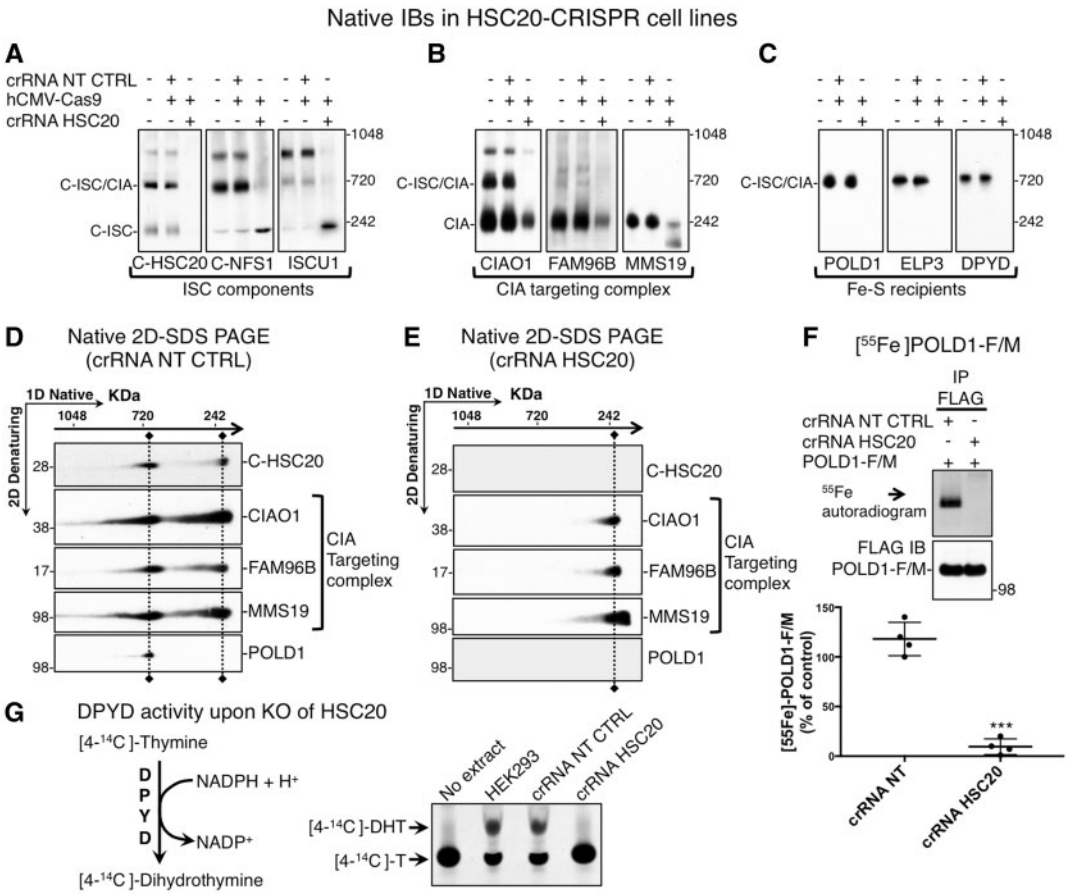

Figure 3. HSC20 is required for formation of a large complex that contains ISC and CIA components and that is essential for Fe-S cluster transfer to several recipients. (**A–C**) Cytosolic fractions from HSC20 KO (crRNA HSC20) or control (crRNA NT CTRL) cell clones were analyzed by native IBs to HSC20, NFS1, ISCU (ISC components), CIAO1, FAM96B, MMS19 (CIA targeting complex) and recipient Fe-S proteins POLD1, ELP3, DPYD to study complex formation between the different components of the Fe-S biogenesis machinery (see main text for a description of the complexes identified). (**D and E**) Cytosolic fractions from control or HSC20 KO cells were subjected to native followed by 2D-SDS-PAGE resolution and IBs to HSC20, CIAO1, FAM96B, MMS19 and POLD1 to investigate complex formation between CIA and ISC components and recruitment of Fe-S recipients upon KO of HSC20. C-ISC indicates the cytosolic ISC complexes. (**F**) ^{55}Fe incorporation into POLD1-FLAG/MYC is abrogated upon KO of HSC20. FLAG IB was performed to verify that equal amounts of POLD1-F/M had been immunoprecipitated. Lower panel, quantification of radioactive iron incorporated into POLD1-F/M shown in the autoradiogram. [^{55}Fe]-POLD1-F/M and POLD1-F/M were quantified and the ratio was normalized to control (crRNA NT CTRL), set to 100%. Values are expressed as % of control and are given as mean ± SEM. $P < 0.001$. (**G**) DPYD-dependent conversion of 4–14C-thymine ([4–14C]-T) to 4–14C-dihydrothymine ([4–14C]-DHT) upon KO of HSC20 (crRNA HSC20), assayed by TLC and autoradiography. The product of DPYD activity [4–14C]-DHT was virtually absent upon KO of HSC20. The reaction mix containing the substrate of the reaction [4–14C]-T without cell extract was loaded as a negative control (no extract) to visualize the substrate (4–14C-thymine) by TLC (A–E, $n = 4$ biological replicates). See also Supplementary Material, Figure S3.

SDS-PAGE confirmed that C-HSC20 was essential for formation of the ISC/CIA complex at 720 kDa, whereas the CIA targeting components CIAO1, FAM96B, MMS19 moderately assembled in the absence of C-HSC20 in the complex at ~242 kDa (compare Fig. 3D, control, and E, HSC20-KO). We next performed functional assays to test the effect of KO of *HSC20* on ^{55}Fe incorporation into POLD1 and on the activity of DPYD. We found that levels of ^{55}Fe levels into POLD1 were dramatically reduced upon KO of *HSC20* (Fig. 3F). DPYD activity was also severely compromised in the absence of HSC20 (Fig. 3G and Supplementary Material, Fig. S3E). Interestingly, ^{55}Fe labeling of the main scaffold protein ISCU1 was increased upon KO of *HSC20*, consistent with the role of the cochaperone in facilitating cluster transfer from ISCU1 to downstream recipients (Supplementary Material, Fig. S3D).

The LYR motif of CIAO1 is required for the interaction with HSC20

We sought to understand how C-HSC20 bridged the ISC and the CIA machineries to form the 720 kDa complex during cytosolic Fe-S cluster biogenesis. Highly conserved residues in the C terminus of mitochondrial HSC20 were reported to mediate its interaction with ISCU2 (15,56) and they are likely involved in recruiting the C-NFS1/ISCU1 complex through direct binding to conserved residues on ISCU1 (Supplementary Material, Fig. S4A). We previously reported that HSC20 is able to bind proteins that contain the Leu Tyr Arg (LYR) sequence to assist Fe-S cluster transfer to recipients (15,31,54). The putative LYR-binding pocket maps to the C terminus of HSC20 and the residues involved in binding LYR-containing peptides are independent from the ISCU binding residues of HSC20, though in

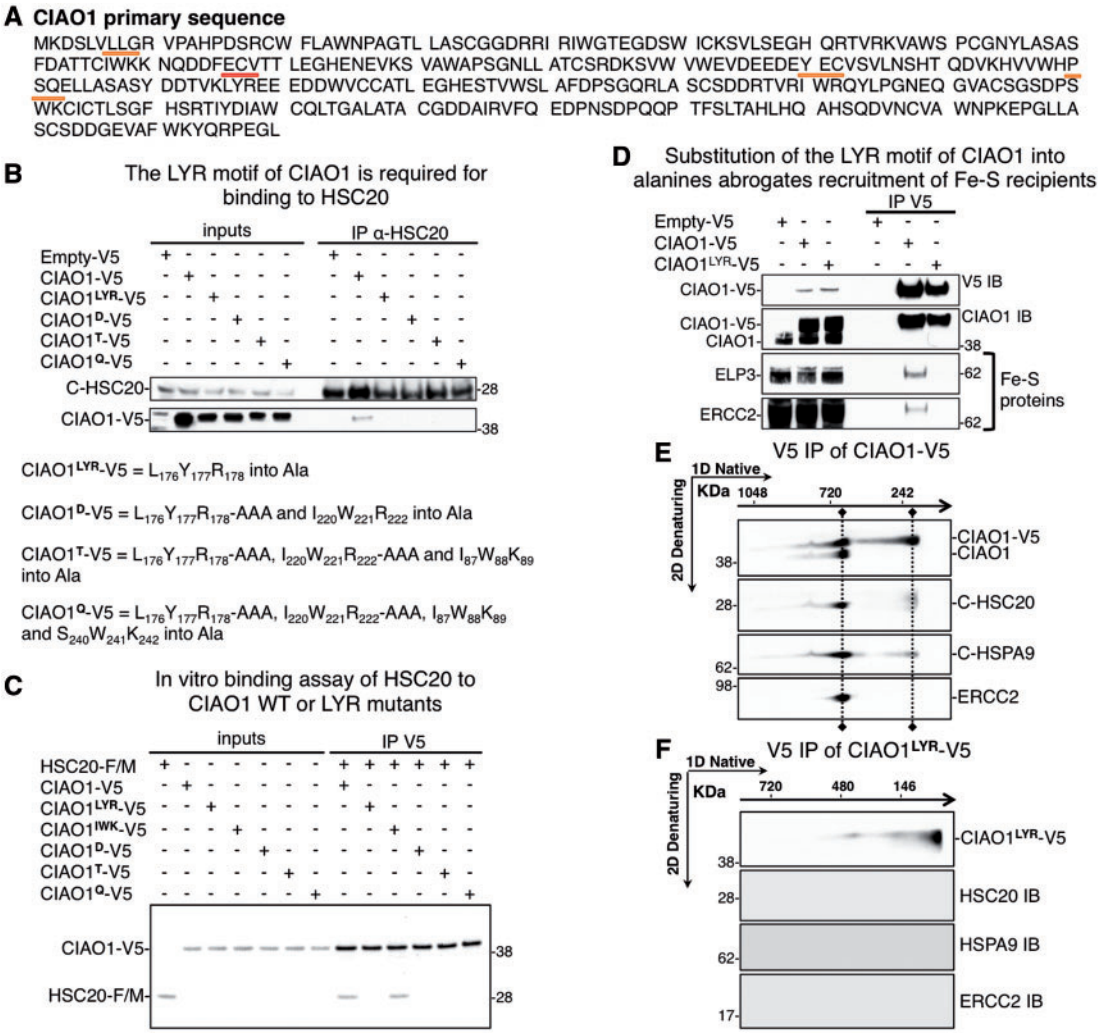

Figure 4. The LYR motif of CIAO1 mediates its binding to HSC20, which is essential for formation of the ISC/CIA complex. (**A**) In the CIAO1 primary sequence, the canonical LYR motif and the LYR-like sequences are highlighted with colored bars above the motifs. (**B**) IP of endogenous C-HSC20 from cytosolic fractions of cells stably expressing CIAO1-V5 WT or the mutants, as indicated. Eluates after IP of C-HSC20 were analyzed by western blot to check for the interaction between CIAO1-V5 WT or mutants and HSC20 (superscript D, T and Q designate the double, triple and quadruple CIAO1 mutants in which substitution of the LYR motif was combined with mutagenesis of one or more LYR-like sequences, as indicated. Empty-V5 is a control cell line, which was stably transfected with the empty vector). (**C**) Pull-down assays of ^{35}S-labeled CIAO1-V5 WT or its mutants, as indicated, were performed in the presence of HSC20-FLAG/MYC (CIAO1^{IWK}-V5 is the mutant in which $I_{87}W_{88}K_{89}$ was replaced by alanines). (**D**) IPs of CIAO1-V5 WT or the $L_{176}Y_{177}R_{178}$ to triple alanine mutant, followed by IBs to V5, CIAO1 and the Fe-S proteins ELP3 and ERCC2. The recipient proteins ELP3 and ERCC2 did not coprecipitate with CIAO1 when the LYR motif of CIAO1 was mutagenized. V5 IPs of CIAO1 WT (**E**) or the LYR mutant (**F**), followed by native and 2D-SDS-PAGE resolution of the competitively eluted cytosolic complexes. IBs to CIAO1, HSC20, HSPA9 and the Fe-S protein ERCC2 are shown (B–F, $n = 4$ biological replicates). See also Supplementary Material, Figure S4.

close proximity (Maio *et al.*, unpublished data). Upon inspection of the primary sequence and three-dimensional structure of CIAO1, we identified one LYR (Leu-Tyr-Arg) motif and three sequences that resembled the LYR consensus sequence (IWK, IWR, SWK, Fig. 4A and Supplementary Material, Fig. S4B). We tested the hypothesis that one or more of these LYR-like sequences interacted directly with HSC20. We generated several stable cell lines that expressed V5-tagged CIAO1 mutants of the $L_{176}Y_{177}R_{178}$ motif or of the other three sequences (IWK, IWR or SWK) (Supplementary Material, Fig. S4C). Additionally, we combined mutagenesis of the LYR motif with substitution of one or more the LYR-like sequences, to generate CIAO1 mutants in which two (in CIAO1^{D}-V5), three (in CIAO1^{T}-V5) or all four (in CIAO1^{Q}-V5) potential motifs were replaced by alanines (Fig. 4B). We found that replacement of $L_{176}Y_{177}R_{178}$ of CIAO1 into triple alanines was sufficient to abolish binding to HSC20 (Fig. 4B). *In vitro* pull-down assays of ^{35}S-labeled CIAO1 wild-type or of the different LYR mutants, in the presence of HSC20 confirmed that the canonical $L_{176}Y_{177}R_{178}$ sequence of CIAO1 was the major molecular mediator of the direct physical interaction with HSC20 (Fig. 4C). Substitution of the LYR-like sequence $I_{87}W_{88}K_{89}$ of CIAO1 into alanines did not affect binding to C-HSC20, consistent with the fact that $L_{176}Y_{177}R_{178}$ mediated the CIAO1/C-HSC20 interaction (Fig. 4C). To further support the requirement of the $L_{176}Y_{177}R_{178}$ of CIAO1 for binding to C-HSC20, we performed IP of V5-tagged CIAO1 wild-type or of the $L_{176}Y_{177}R_{178}$ mutant proteins and analyzed the eluates by 2D-SDS PAGE and immunoblots. The results confirmed that substitution of $L_{176}Y_{177}R_{178}$ of CIAO1 into alanines abrogated binding to HSC20 and formation of the C-ISC/CIA complex at 720 kDa (Fig. 4E and F), thereby impairing recruitment and biogenesis of Fe-S recipients (ERCC2 is shown as a representative

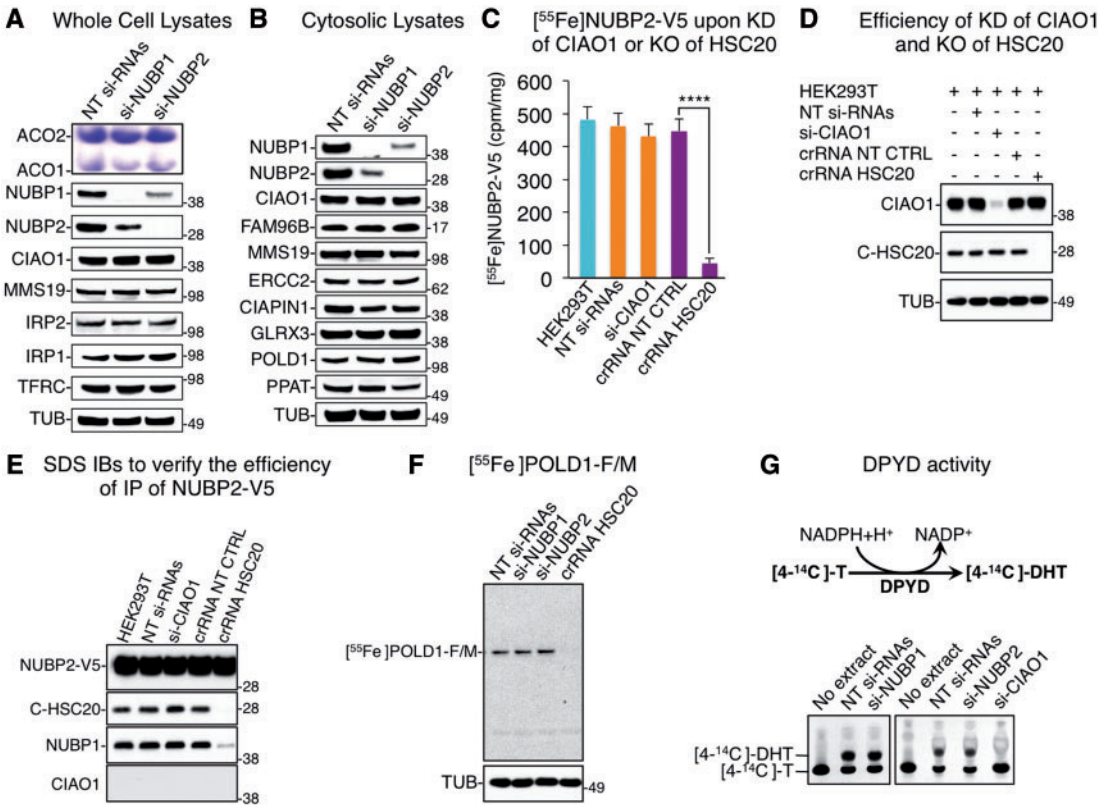

Figure 5. A pathway to transfer nascent clusters to a subset of cytoplasmic and nuclear proteins was identified, which was not mediated by the NUBP1/NUBP2 complex. (**A**) Total lysates after 6 days of KD of NUBP1 and NUBP2 were assayed for in-gel aconitase activities (ACO2 is mitochondrial aconitase, ACO1 is cytosolic aconitase), or analyzed by western blot to assess efficiency of KD of NUBP1 and NUBP2, and levels of CIAO1, MMS19, iron-regulatory proteins IRP1 and IRP2, and transferrin receptor TFRC. Tubulin (TUB) was used as a loading control (NT si-RNAs, nontargeting si-RNAs). (**B**) Cytosolic fractions after 6 days of KD of NUBP1 or NUBP2 were analyzed by western blot to check levels of NUBP1, NUBP2, CIAO1, FAM96B, MMS19, and the Fe-S proteins ERCC2, CIAPIN1, GLRX3, POLD1 and PPAT. (**C**) ^{55}Fe incorporation into NUBP2-V5 upon KD of CIAO1 (si-CIAO1) or KO of HSC20 (crRNA HSC20). (crRNA NT CTRL is a scramble CRISPR RNA used as negative control). Only KO of HSC20 significantly reduced ^{55}Fe incorporation into NUBP2-V5. Values are given as mean ± SD. CrRNA NT CTRL versus crRNA HSC20, $P < 0.0001$. (**D**) IBs on cytosolic fractions from cells upon KD of CIAO1 (si-CIAO1) or KO of HSC20 (crRNA HSC20). Tubulin was used as a loading control. (NT si-RNAs, nontargeting si-RNAs; crRNA NT CTRL, scramble CRISPR RNA). (**E**) IBs to V5, HSC20, NUBP1 and CIAO1 on eluates after IP of V5-tagged NUBP2 from cytosolic fractions of control cells or of cells transfected with si-RNAs to KD CIAO1 or of HSC20 KO cell clones. (**F**) ^{55}Fe incorporation into POLD1-FLAG/MYC upon KD of NUBP1, NUBP2 or KO of HSC20. Neither loss of NUBP1 or NUBP2 diminished ^{55}Fe incorporation. (**G**) DPYD-dependent conversion of 4–14C-thymine ([4–14C]-T) to 4–14C-dihydrothymine ([4–14C]-DHT) upon KD of NUBP1, NUBP2 or CIAO1, assayed by TLC and autoradiography. The product of DPYD activity [4–14C]-DHT was virtually absent only upon KD of CIAO1, whereas it was not affected by KD of NUBP1 or NUBP2. The reaction mix containing the substrate of the reaction [4–14C]-T without cell extract was loaded as a negative control (no extract) to visualize the substrate (4–14C-thymine) by TLC (A–G, $n = 6$ biological replicates). See also Supplementary Material, Figure S5.

Fe-S client in Fig. 4D–F). The inability of the $L_{176}Y_{177}R_{178}$ mutant of CIAO1 to interact with C-HSC20 led to the unusual migration of the mutant in a complex with lower MW compared with wild-type CIAO1 (compare Fig. 4F to E).

Transfer of Fe-S clusters to a subset of cytoplasmic and nuclear proteins was not mediated by NUBP1 and NUBP2

Our proteomic and biochemical data implied that the scaffold protein ISCU1 was essential for *de novo* Fe-S cluster biogenesis in the cytosol on the basis of its interactions with C-NFS1, C-HSC20 and the CIA targeting complex, and on functional studies with the dominant negative mutant ISCU1^{D46A}. Therefore, we decided to interrogate the role of a cytosolic complex, composed of NUBP1 and NUBP2 dimers, which was previously proposed to function as the primary scaffold in cytosolic Fe-S biogenesis (57,58). We found that effective knock down (KD) of NUBP1 or NUBP2 for 6 days had no significant effect on the activity of cytosolic aconitase (ACO1) or on the stability of several Fe-S proteins tested (i.e. ERCC2, CIAPIN1, GLRX3, POLD1, PPAT) (Fig. 5A and B and Supplementary Material, Fig. S5A and B). Interestingly, ^{55}Fe incorporation into NUBP2-V5 was significantly diminished upon KO of HSC20, whereas it was not affected by KD of CIAO1 (Fig. 5C), consistent with previous studies that showed that NUBP1 and NUBP2 acted upstream of the CIA targeting complex and did not interact with its components (57–60). Formation of the NUBP1/NUBP2 complex was also significantly decreased upon KO of HSC20 (Fig. 5E, crRNA HSC20). Our data confirmed that NUBP1 and NUBP2 did not interact with the CIA targeting complex. Additionally, we found that NUBP2 depended on HSC20 to acquire its Fe-S cluster (Fig. 5C).

^{55}Fe incorporation into POLD1 was unchanged upon KD of NUBP1 or NUBP2 (Fig. 5F and Supplementary Material, Fig. S5C), whereas it was markedly reduced upon KO of HSC20 (Fig. 5F and Supplementary Material, Fig. S5C). DPYD activity was also unaffected by KDs of NUBP1 or NUBP2, whereas it was significantly decreased upon KD of CIAO1 (Fig. 5G and Supplementary Material, Fig. S5D). Because KO of HSC20 by CRISPR is more efficient than the si-RNA mediated KDs of NUBP1 and NUBP2,

we compared the effects of KD of NUBP1, NUBP2 or HSC20 for 6 days on the levels of radioactive iron incorporated into POLD1. We found that ^{55}Fe incorporation into POLD1 was unchanged upon KD of NUBP1 or NUBP2 (Fig. 5F and Supplementary Material, Fig. S5C), whereas it was markedly reduced upon KD of HSC20 (Supplementary Material, Fig. S5E), suggesting that NUBP1/2 were not involved in the biogenesis of the Fe-S prosthetic group of POLD1. Overall, these data suggest that NUBP1 and NUBP2 are not involved in the biogenesis of Fe-S clusters for either cytosolic aconitase (ACO1, Fig. 5A and Supplementary Material, Fig. S5A and B), POLD1 (Fig. 5F and Supplementary Material, Fig. S5C) or DPYD (Fig. 5G and Supplementary Material, Fig. S5D). Our results are in contrast with the proposed role of NUBP1/NUBP2 as the main scaffold complex from which all cytosolic and nuclear Fe-S proteins acquire their clusters (57–59). In previous reports that examined the effect of KD of NUBP1 or NUBP2 on cytosolic aconitase activity, cells were retransfected multiple times with si-RNAs and grown for up to 9 or 15 days to see a significant effect on ACO1 activity or on protein levels of PPAT (58,61). In our studies, we obtained efficient knockdowns of NUBP1 and NUBP2 after only 3 days from the initial si-RNA-mediated transfections, with undetectable levels of the two proteins in western blot (data not shown). We analyzed the effects of KDs of NUBP1 and NUBP2 after 6 days from the initial transfection (cells were retransfected overall twice with si-RNAs in the 6-day period), when the levels of NUBP1 and NUBP2 had been effectively depleted (as the proteins were undetectable by western blots in Fig. 5A and B), without incurring the general cellular morbidity caused by KDs prolonged for 9 or 15 days. We did not find significant changes in the activity, stability or iron incorporation of the Fe-S proteins tested (Fig. 5A, B, F and G and Supplementary Material, Fig. S5A–E). Conversely, KD of HSC20 over the same time period significantly decreased iron incorporation into POLD1 (Supplementary Material, Fig. S5E). The studies that favor the role of NUBP1/NUBP2 as the main cytosolic scaffold complex failed to explain how Fe-S clusters are transferred from these two P-loop NTPases to the CIA targeting complex and ultimately to recipient Fe-S proteins, given the vulnerability of Fe-S clusters to oxidative damage, which requires that Fe-S clusters remain ligated and protected during all the steps of the biogenesis process. On the basis of the data presented here, we propose that a *de novo* Fe-S biogenesis pathway operates in the cytosol of mammalian cells to assemble, escort and deliver Fe-S clusters to cytoplasmic and nuclear Fe-S proteins. The cytosolic ISC machinery consists of cytosolic isoforms of the main components that function in mitochondria and relies on the cochaperone HSC20 for recruiting the CIA targeting complex during cytosolic Fe-S cluster biogenesis.

Discussion

In the present study, we investigated the potential role of the cochaperone HSC20 in the biogenesis of Fe-S clusters in the cytosol of mammalian cells. By using a combination of proteomic and biochemical approaches, we identified a cytosolic pathway analogous to the mitochondrial biogenesis pathway by which HSC20 facilitates Fe-S cluster transfer to cytoplasmic and nuclear recipients. The cytosolic Fe-S biogenesis pathway relies on the initial assembly of the nascent cluster on ISCU1 (Fig. 6, step 1), by the coordinated action of a multimeric complex in which the cytosolic isoform of the cysteine desulfurase, C-NFS1, is the enzyme that mobilizes sulfur for initial cluster formation on ISCU1. The HSC20/HSPA9 cochaperone/chaperone system interacted with ISCU1 (Fig. 6, step 3) and appeared to facilitate direct cluster transfer to a subset of cytosolic Fe-S proteins, including NUBP1, NUBP2 and GLRX3 (Fig. 6, step 4a). Alternatively, a subset of Fe-S proteins involved in DNA metabolism acquired their clusters through the action of a large multisubunit C-ISC/CIA complex (Fig. 6, step 4b). In the CIA-mediated Fe-S transfer mechanism, C-HSC20 bridged components of the initial biogenesis pathway, ISCU1, NFS1, HSPA9, to the CIA targeting complex, consisting of CIAO1, FAM96B and MMS19 into a 720 kDa ISC/CIA multiprotein complex. Functional assays demonstrated that in the absence of C-HSC20, several Fe-S proteins, including POLD1, DPYD, NUBP2, ERCC2, ELP3 and PPAT failed to acquire their clusters. Similarly, we detected that the levels of multiple cytoplasmic and nuclear Fe-S proteins dramatically declined upon induction of expression of a dominant negative mutant of the cytosolic isoform of the main scaffold ISCU1 (ISCU1^{D46A}). ISCU1 wild-type and the ISCU1^{D46A} specifically localized to the cytosol of mammalian cells, demonstrating that damage to cytosolic Fe-S proteins upon expression of ISCU1^{D46A} was not indirectly caused by impairment of the mitochondrial ISC biogenesis pathway. The ISCU1^{D46A} mutant remained trapped in complex with the cysteine desulfurase, similar to the bacterial orthologs of the IscU Asp into Ala mutants (51–53). KO of *HSC20* or expression of ISCU1^{D46A} resulted in similar phenotypes and loss of Fe-S proteins because both genetic manipulations halted the biogenesis pathway to the step of Fe-S cluster formation on ISCU1 and impaired transfer to downstream recipients. Our data also showed that efficient KD of NUBP1 or NUBP2 did not affect stability of Fe-S recipient proteins, or the activities of DPYD and cytosolic aconitase, or Fe-S cluster acquisition by POLD1, in contrast with previous reports indicating a role of NUBP1 and NUBP2 as upstream Fe-S scaffolds (57,58).

On the basis of our data, we propose that C-HSC20 functions as a crucial intermediary between the portion of the core Fe-S biogenesis machinery that localizes to the cytosol of mammalian cells (C-ISC), the CIA targeting complex and recipient Fe-S proteins. Our data suggest that the CIA targeting complex functions in Fe-S transfer when it is incorporated in a 720 kDa complex which contains ISC components that are tethered by dimerization of HSC20 to a second HSC20 that binds CIAO1 through its LYR motif (Fig. 6, steps 3 to 4b). Molecular details of how components of the ISC and CIA machineries coordinate their functions within the 720 kDa complex to efficiently transfer Fe-S clusters to recipient proteins remain to be investigated.

Nuclear genome instability has been linked to defects in Fe-S cluster biogenesis since 2009 (62). In the study from Veatch and colleagues, nuclear genome instability was proposed to occur because of a defect in mitochondrial Fe-S cluster biogenesis. The dependence on mitochondrial biogenesis was based on genetic studies conducted in yeast, which proposed that assembly of Fe-S clusters for nuclear proteins, while primarily taking place in the cytoplasm, depends on the mitochondrial Fe-S biogenesis machinery for the synthesis of a sulfur-containing compound that is exported to the cytosol by the ABC transporter Atm1 (ABCB7 in human) and utilized by the CIA machinery for Fe-S cluster assembly (16). However, the indirect evidence that suggested that Atm1 exports Fe–S clusters from mitochondria should be analyzed with caution. The yeast strain lacking Atm1 had low levels of activity of the cytosolic Fe–S protein Leu1, which is part of the leucine biosynthetic pathway of yeast (16). Selective inactivation of *Atm1* was achieved by using a plasmid that reintroduced functional Leu2 into a Leu2-null strain. It is now known that when Leu biosynthesis is low due to defects in either Leu1 or Leu2, the regulatory gene *Leu3* upregulates the

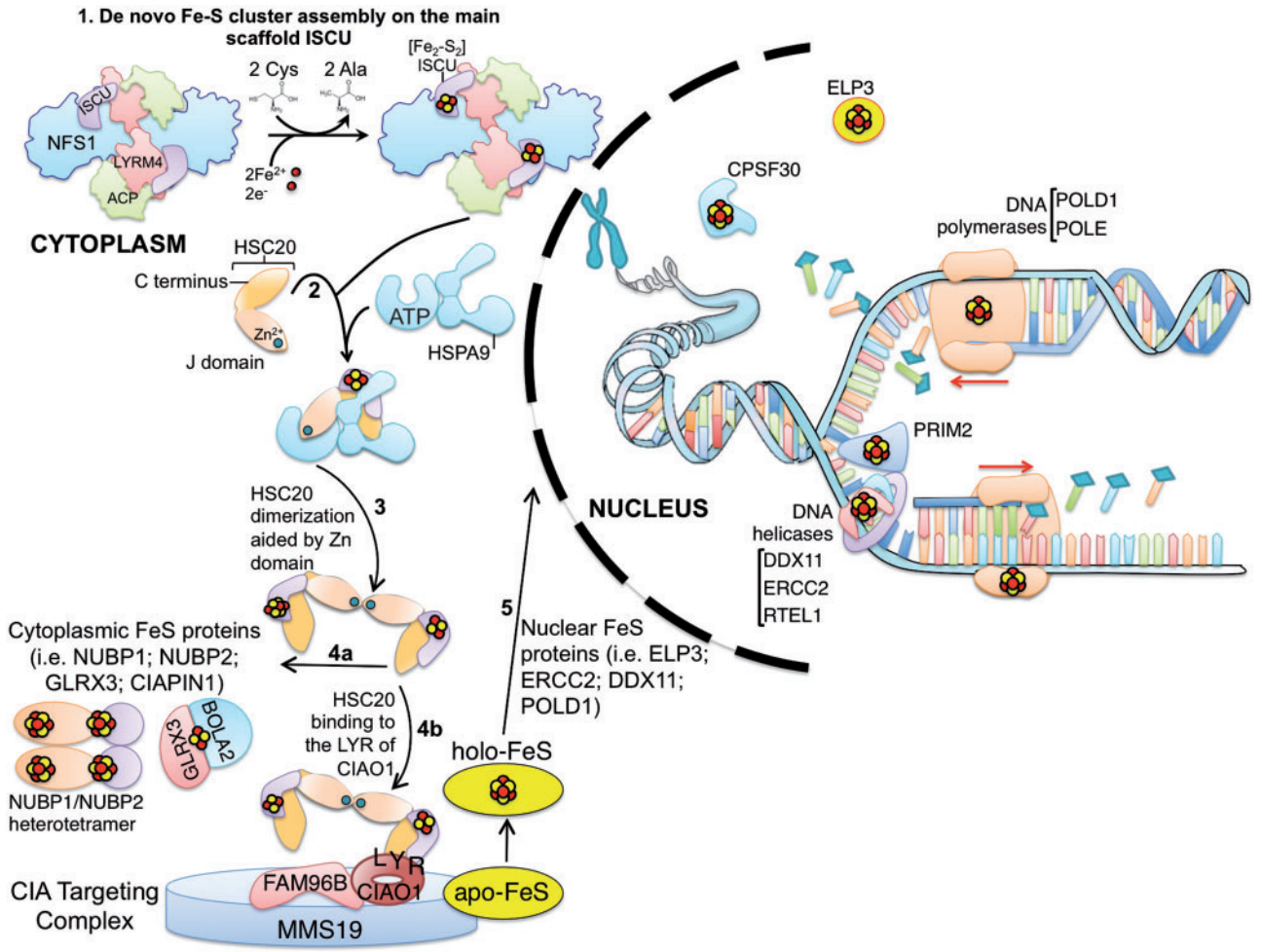

Figure 6. Proposed model of the biogenesis of Fe-S clusters in the cytosol of mammalian cells. **1.** *De novo* biogenesis of Fe-S clusters occurs in the cytosol of mammalian cells upon the main scaffold protein ISCU1 by the concerted action of a multimeric complex, which consists of the cytosolic cysteine desulfurase NFS1 and the accessory protein LYRM4 (model on the basis of the recently solved crystal structure of the eukaryotic complex, which identified also the ACP, as part of the complex (11)). **2.** The HSC20/HSPA9 cochaperone/chaperone system interacts with ISCU1 to facilitate cluster transfer to multiple recipients. **3.** The functional unit of HSC20 is a dimer, as impairing HSC20 dimerization abrogates the network of interactions necessary for cytosolic Fe-S cluster biogenesis. **4a.** A subset of recipient Fe-S proteins acquire their clusters directly from the HSC20/HSPA9/ISCU1 complex, as their biogenesis is independent from the CIA targeting complex. **4b.** Binding of HSC20 to the LYR motif of CIAO1 recruits the CIA targeting complex, which is known to form a platform to which Fe-S recipients involved in DNA metabolism dock to acquire their clusters prior to their translocation to the nucleus (5). The Fe-S proteins shown in the model were all identified as C-HSC20 interacting partners in our studies (i.e. NUBP2, GLRX3, CIAPIN1, ABCE1, ERCC2, POLD1, PRIM2, PPAT, ELP3, CPSF30, DDX11, etc.).

transcription of genes encoding both Leu1 and Leu2 to correct for Leu deficiency (63). Thus, transcript levels of *Leu1* were extremely high in the *Leu2*-deficient strain that expressed normal Atm1 (63), and Leu1 enzymatic activity was accordingly high. Higher Leu1 activity in the Atm1-sufficient cells was interpreted to mean that Atm1 exports the Fe–S cluster that is incorporated into cytosolic Leu1. However, when yeast strains were re-examined with matching *Leu2* genes, Leu1 activity was not influenced by Atm1 overexpression or depletion (63). Therefore, the conclusions on the basis of the use of the Leu2-null/Atm1-null strain should be interpreted with caution. The human ortholog of yeast Atm1 is the ATP-binding cassette transporter ABCB7. Mutations in *ABCB7* cause sideroblastic anemia with ataxia in human and the gene was shown to be essential for hematopoiesis in conditional KO mouse models of *Abcb7* (64,65). KD of ABCB7 in cell culture models was shown to cause mitochondrial iron overload and decreased mitochondrial (ACO2) and cytosolic (ACO1) aconitase activities (ACO2 was 50% of control and ACO1 was 40% of control) (66), consistent with results obtained in yeast upon depletion of *Atm1* (67).

The effect of mitochondrial dysfunction on genome instability, rather than being caused by the impaired export of the sulfur compound for biogenesis of Fe-S proteins involved in DNA processing in the cytosol, can reasonably be explained by the fact that several enzymes of the metabolic pathways responsible for the biosynthesis of cytosolic ribo- and deoxyribonucleotides are located in mitochondria and the rate limiting steps of these processes are known to be affected by mitochondrial function (68). Importantly, C-NFS1 is a functional sulfur mobilizing enzyme (26,50), a notion that questions the need for the export of a sulfur containing compound out of mitochondria.

Fe-S proteins are present in all subcellular compartments of eukaryotic cells, where they perform essential functions. Despite a high degree of sequence homology of the ISC

components from bacteria to human, and common basic molecular pathways for Fe-S biogenesis, increased biological complexity in multicellular organisms evolved with a corresponding demand for more elaborate mechanisms of transcriptional/translational control, along with a greater diversity in the multisubunit complexes that facilitate Fe-S cluster assembly in different compartments. Alternative isoforms sorted to different subcellular compartments provide a control mechanism to regulate similar biological processes in different cellular sites (69,70). Importantly, alternative isoforms of the components of the ISC machinery that operates in mitochondria, including the cysteine desulfurase NFS1 and its interacting partner ISD11, the main scaffold ISCU, the secondary carrier NFU and the cochaperone HSC20, have been identified in the cytosolic and nuclear compartments of mammalian cells (14,15,20–25), suggesting that Fe-S cluster biogenesis machineries may independently operate in parallel to generate nascent Fe-S clusters in multiple subcellular compartments of multicellular eukaryotes. The inherent reactivity of Fe-S clusters toward a variety of redox-active species makes them irreplaceable cofactors in several crucial enzymes, but it is also the cause of their vulnerability. Any of the reactions in which Fe-S cluster cofactors are involved may result in a change in the redox state of the cluster, cluster conversion or even complete cluster loss. It seems therefore rather intuitive that the Fe-S assembly pathway may have evolved as a compartmentalized process, which assures that Fe-S clusters are chaperoned and tethered to recipient proteins or to intermediate carriers throughout their biogenesis process. Here, we demonstrated that the cytosolic Fe-S assembly pathway is functional and that it is required for biogenesis of cytoplasmic and nuclear Fe-S proteins. Fe-S clusters are essential cofactors in enzymes involved in all aspects of DNA processing (71). In addition to providing insights into fundamental aspects of Fe-S protein assembly, our studies may have implications for understanding the molecular basis of diseases associated with genome instability (39–41), and of the increasing number of human diseases caused by defects in the Fe-S biogenesis factors (9,35,72,73).

Materials and Methods

Contact for reagent and resource sharing

Correspondence and requests for materials should be addressed to and will be fulfilled by Tracey A. Rouault (rouault@mail.nih.gov).

Cell lines and cell culture conditions

HEK293, HEK293T and HeLa cells were purchased from ATCC. Cells were propagated in Dulbecco's modified Eagle's medium (DMEM) with 4.5 g/l glucose, supplemented with 10% fetal bovine serum (FBS) and 2 mM glutamine at 37°C and 5% CO_2 in a humidified incubator. HSC20-knockout cell clones were propagated in DMEM with 4.5 g/l glucose supplemented with 10% FBS, 2 mM glutamine, 1 mM sodium pyruvate, 50 μg/ml uridine. All cell lines were subjected to mycoplasma testing.

Method Details

Plasmids and transfection of human cells

Plasmids used for transient expression in human cells were all pCMV6-Entry-based (Origene) to allow expression from a CMV-promoter. Several versions of the pCMV6-Entry backbone vector containing different epitope tags in frame at the 3′ of ORFs encoding the genes of interest were generated for different experiments. Point mutations were introduced using the QuikChange II site-directed mutagenesis kit (Agilent Technologies), following the manufacturer's instructions. Plasmid transfections into human cells were performed with Lipofectamine 2000 (Thermo Fisher Scientific), according to standard procedures.

Stable cell lines expressing either ISCU1-MYC or ISCU1^{D46A}-MYC were generated using the Lenti-X^{TM} Tet-On$^{®}$ 3G Inducible Expression System (Clontech), according to the manufacturer's instructions. Briefly, HEK293 cells were transfected with pLVX-TetOne harboring the ORF of *ISCU1* wild-type or mutant under the control of a doxycycline-inducible promoter.

The stable cell line expressing CIAO1-V5 was generated by cloning the *CIAO1* ORF into pLENTI6.2/V5-DEST (Invitrogen). The ViraPower Lentiviral Expression System (Invitrogen) was used to produce viral particles harboring *CIAO1-V5* under the control of a CMV promoter, according to the manufacturer's instructions. Briefly, pLENTI6.2/CIAO1-V5 was cotransfected with the ViraPower Packaging Mix into HEK293T cells. The lentiviral stock collected 36 h after cotransfection was used to transduce HeLa cells. Stable clones were established after 6 days of selection with blasticidin. Expression levels of CIAO1-V5 were assessed by western blot.

Stable cell lines expressing the CIAO1-V5 mutated versions in which the $L_{176}Y_{177}R_{178}$ motif or one or more of the other three LYR-like sequences (IWK, IWR or SWK) were replaced by alanines were generated by introducing point mutations into pLENTI6.2/CIAO1-V5 using the QuikChange II site-directed mutagenesis kit (Agilent Technologies), followed by packaging of the viral particles and transduction of the mutated *CIAO1* genes into HeLa cells. Stable clones were established after 6 days of selection with blasticidin. Expression levels of CIAO1-V5 mutated proteins were assessed by western blot.

Si-RNA transfection of human cells

On-TARGETPlus si-RNA pools against human *CIAO1* (L-019857–00-0005), *NUBP1* (L-019603–00-0005), *NUBP2* (L-004705–00-0005) and the control non-targeting pool (D-001810–10-05) were purchased from Dharmacon.

ON-TARGETPlus Human *CIAO1* siRNA Target Sequences:

GUGCGUAUCUGGCGUCAGU

GGAAGAGGAUGACUGGGUA

CAGUGAAGCUGUACCGGGA

GGAAAUGUAUCUGUACUUU

ON-TARGETPlus Human *NUBP1* siRNA Target Sequences:

GCUCAUAGGUAAGAAUUGU

GGACACGGCUAUAGAGGAA

GAAAUCAACUUCUGCCGCA

ACACAUCGAUGGAGCAGUG

ON-TARGETPlus Human *NUBP2* siRNA Target Sequences:

GCUUGCGGGUGAUGGGAAU

UAAAGCAGUUUGUGUCCGA

GAGCUGACCUUCUGUAGGA

ON-TARGETPlus Human non targeting siRNA Target Sequences:

UGGUUUACAUGUCGACUAA

UGGUUUACAUGUUGUGUGA

UGGUUUACAUGUUUUCUGA

UGGUUUACAUGUUUUCCUA

KD of the gene of interest was achieved by transfecting cells twice with siRNAs at a 48-h interval using Dharmafect 1 according to the manufacturer's instructions. Cell lysates were analyzed at the time points specified in the main text or figure legends.

CRISPR knockout

For the knockout of *HSC20*, 1.5×10^5 HeLa cells in 24-well were transfected with 50 nM of the trans-activating CRISPR RNA (tracrRNA): human *HSCB* CRISPR RNA (crRNA) and 1 μg/well of Cas9 expression plasmid (Edit-R hCMV-PuroR-Cas9 Expression Plasmid, Dharmacon) using Dharmafect Duo Transfection Reagent (Dharmacon). As a negative control, cells were cotransfected with a nontargeting crRNA (NT crRNA, U-007501, Dharmacon) and 1 μg/well of Cas9 expression plasmid. We used the guide sequence *CCTGCAGCGCTCGGCACTGT* to target exon 1 of human *HSCB* gene (exon target list: NM_172002). Forty-eight hours after transfection, cells were passed, and puromycin selection was started 24 h later. Cells were incubated in selection medium for additional 4 days. Purified genomic DNA from single cell colonies was analyzed with the mismatch detection assay SURVEYOR Mutation Detection kit (Integrated DNA Technologies) for identification of indels in the cell populations. The following primers were used to generate the 625 bp PCR amplicons of the *HSC20* gene that were subjected to Surveyor Nuclease S digestion at 42°C for 30 min:

Forward: 5′-AGATAGGCCGCCGGCCAGATGTGG-3′

Reverse: 5′-GTACTTGAGGGGCAGGGCCTGG-3′

PCR products of wild-type and mutated DNA were hybridized, allowing individual DNA strands to reassort. Incubation with the Surveyor nuclease cleaved the resulting base mismatches in the cell populations that had undergone editing. The digestion products were electrophoresed; cleavage products of 397 and 228 bp were only seen in the HSC20-KO cell clones.

After Sanger sequencing, the cell clones which had undergone editing were analyzed for HSC20 expression by western blot.

Cell fractionation, IP and MS

Whole cell lysates were prepared in lysis buffer I: 25 mM Tris, 0.15 M NaCl, 1 mM ethylenediaminetetraacetic acid (EDTA), 1% Nonidet P-40, 5% glycerol (pH 7.4), protease and phosphatase inhibitor cocktail with no EDTA (Roche).

Cytosolic fractions were isolated from HeLa, HEK293 or stable cell lines after permeabilization with a buffer containing 0.1% digitonin in 210 mM mannitol, 20 mM sucrose and 4 mM HEPES. The supernatants after the first centrifugation step at 700*g* for 5 min were subjected to 20 000*g* for 15 min. The supernatants after the second centrifugation step were saved as cytosolic (soluble) fractions.

IPs were done on cytosolic fractions from HEK293, HeLa or the stable cell lines, as indicated. Anti-FLAG IPs were performed using M2-FLAG beads (Sigma). Washed FLAG M2 beads were added to the lysate and incubated for 2 h at room temperature. Beads were recovered after extensive washing, and proteins were eluted with Tris-Glycine pH 2.8 (elution buffer, EB), or for the native elution, protein complexes were competitively eluted with 100 μg/ml 3xFLAG peptide (Sigma). Anti-V5 IPs were performed using V5 agarose beads (Sigma). Anti-MYC IPs were performed using MYC agarose beads prepared by covalently coupling anti-MYC antibody produced in mouse (Sigma-Aldrich) onto an amine-reactive resin (Pierce Co-IP kit, Cat. No. 26149), following the manufacturer's instructions. IP of endogenous HSC20 was done by covalently coupling anti-HSC20 antibody produced in rabbit (Sigma-Aldrich) onto an amine-reactive resin (Pierce Co-IP kit, Cat. No. 26149), following the manufacturer's instructions. IP with antirabbit IgG was used as negative control. Lysates from cytosolic fractions were incubated with the beads overnight at 4°C, and then washed extensively with lysis buffer I. Bound proteins were eluted with Tris-Glycine pH 2.8 for 10 min at 4°C. Aliquots corresponding to 10–15% of cytosolic lysates were run alongside the IP fractions onto the gels as inputs. IP of endogenous NFS1 was done by covalently coupling anti-NFS1 antibody produced in mouse (Santa Cruz Biotechnology) onto an amine-reactive resin (Pierce Co-IP kit, Cat. No. 26149), following the manufacturer's instructions. IP with antimouse IgG was used as negative control. Lysates from cytosolic fractions were incubated with the beads overnight at 4°C, and then washed extensively with lysis buffer I. Bound proteins were eluted with Tris-Glycine pH 2.8 for 10 min at 4°C. Aliquots corresponding to 10–15% of cytosolic lysates were run alongside the IP fractions onto the gels as inputs.

For MS analysis, three biological replicates of the eluates after IP of endogenous HSC20 or NFS1 on cytosolic extracts were independently precipitated using trichloroacetic acid (TCA), washed with acetone, air-dried and analyzed by liquid chromatography (LC)/MS at the Taplin MS facility (Harvard Medical School). Only proteins that specifically copurified with C-HSC20 in the IPs with antirabbit HSC20 antibody or with C-NFS1 in the IPs with antimouse NFS1 antibody and not in the negative controls (antirabbit or antimouse IgGs, respectively) were considered for further analysis. Briefly, TCA precipitates were digested in 100 μl of 50 mM ammonium bicarbonate with ~2 ng/μl of trypsin overnight. Peptides were then extracted by removing the ammonium bicarbonate solution, followed by one wash with a solution containing 50% acetonitrile and 1% formic acid. The extracts were then dried in a speed-vac, reconstituted in 5–10 μl of high-performance liquid chromatography (HPLC) solvent A (2.5% acetonitrile and 0.1% formic acid), and loaded into a nano-scale reverse-phase HPLC capillary column via a Famos auto sampler (LC Packings, San Francisco, CA). A gradient was formed and peptides were eluted with increasing concentrations of solvent B (97.5% acetonitrile and 0.1% formic acid). As peptides eluted they were subjected to electrospray ionization and then entered into an LTQ Velos ion-trap mass spectrometer (ThermoFisher, San Jose, CA). Peptides were detected, isolated and fragmented to produce a tandem mass spectrum of specific fragment ions for each peptide. Peptide sequences (and hence protein identities) were determined by matching the *H. sapiens* Uniprot database with the acquired fragmentation pattern by the software program, Sequest (Thermo Fisher Scientific) (74). Databases included a reversed version of all the sequences, and consensus identification lists were generated with FDRs of 1% at protein and peptide levels.

In vitro coupled transcription/translation and pull down assay of ^{35}S-labeled proteins

The TNT Quick Coupled Transcription/Translation system (Promega), which couples transcription/translation reactions for

in vitro synthesis of eukaryotic proteins starting with plasmid DNA as a template (1 μg of DNA/reaction), was used to synthesize ^{35}S-labeled proteins for pull-down assays. About 20 μCi of [^{35}S]-methionine/cysteine (EasyTag™ EXPRESS35S Protein Labeling Mix stabilized aqueous solution from PerkinElmer) was added to the reaction mix and the incubation was performed at 30°C for 3 h. Pull down assays of ^{35}S-labeled V5-tagged proteins (CIAO1-V5 wild-type or mutants) were done in the presence of the ^{35}S-labeled FLAG/MYC-tagged HSC20. Binding was performed in buffer I2 (25 mM Tris–HCl; 300 mM NaCl; 1 mM EDTA; 1% Nonidet P-40; 1% dithiothreitol; 1 mM PMSF; 5% glycerol) at room temperature for 3 h, using anti-V5 antibody (Sigma) covalently bound to beads to immunoprecipitate CIAO1-V5 tagged proteins. The presence of coeluted HSC20-FLAG/MYC was analyzed by SDS-PAGE and autoradiogram. Aliquots corresponding to 20–30% of the inputs were run on the gel for comparison.

Native PAGE (BN-PAGE) and native immunoblots

The NativePAGE Novex Bis-Tris gel system (Thermo Fisher Scientific) was used for the analysis of native cytosolic protein complexes, with the following modifications: only the Light Blue Cathode Buffer was used; 20 μg of cytosolic protein extracts were loaded/well; the electrophoresis was performed at 150 V for 1 h and 250 V for 2 h. For the native IB, PVDF was used as the blotting membrane. The transfer was performed at 25 V for 3 h at 4°C. After transfer, the membrane was washed with 8% acetic acid for 20 min to fix the proteins, and then rinsed with water before air-drying. The dried membrane was washed five to six times with methanol (to remove residual Coomassie Blue G-250), rinsed with water and then blocked for 2 h at room temperature in 5% milk, before incubating with the desired antibodies diluted in 2.5% milk overnight at 4°C. To avoid strip and reprobing of the same membrane, which might cause detection of signals from the previous IBs, samples were loaded and run in replicates on adjacent wells of the same gel, and probed independently with different antibodies.

Two-dimensional native/SDS-PAGE

Two-dimensional native/SDS-PAGE was performed by resolving the cytosolic protein complexes in the first dimension, by BN-PAGE. Each lane of the gel was excised, equilibrated in SDS buffer supplemented with reducing agent, and then immersed in the alkylating solution for 15 min, before quenching for additional 15 min. For the second dimension, the gel strip was fixed horizontally onto the NuPAGE 4–12% Bis–Tris Zoom Gel (Thermo Fisher Scientific), and classical SDS immunoblots were performed.

DPYD activity

The DPYD activity was determined by thin layer chromatography (TLC), following a previously described protocol (38), with the following modifications. Cell lysates containing 150 μg of proteins isolated from control, KD or KO cell lines, as specified in the main text and figure legends, were applied to 50 μl of a reaction mix containing 25 mM Tris–HCl (pH 7.5), 0.1% digitonin, 2.5 mM $MgCl_2$, 2 mM DTT, 10 μM [4–14C]-thymine (0.1 mCi/ml, Moravek Inc., CA, USA), 10 mM NADPH. After 4 h of incubation at 32°C, the reaction was stopped by addition of 10 μl of perchloric acid (10%, v/v). Reaction mixtures were centrifuged at 20 000*g* for 5 min and the supernatants analyzed by TLC.

Iron incorporation assay

The ^{55}Fe incorporation assays were performed essentially as previously described (15,54), with minor modifications. Cells were grown in the presence of 1 μM ^{55}Fe-Tf for 5–7 days. Cytosolic extracts were subjected to IP with anti-FLAG to immunocapture POLD1-FLAG. Anti-MYC IPs were performed to immunoprecipitate ISCU1-MYC wild-type or the D46A mutant, and anti-V5 IPs were carried out to isolate NUBP2-V5. Samples collected after competitive elution (with 3X FLAG, MYC or V5 peptides) were run on a native gel, followed by autoradiogram.

Alternatively, ^{55}Fe incorporation into NUBP2-V5 was measured by scintillation counting of V5-beads after immunoabsorption of NUBP2-V5, followed by extensive washings with buffer I. The background, corresponding to ^{55}Fe measurements of eluates after anti-V5 IPs on cytosolic extracts from cells transfected with the empty vector was subtracted from each reading.

Immunoblots

Antibodies in these studies were as following: Anti-CIAO1 (sc-374498), NFS1 (sc-81107) and DPYD (sc-376681) were from Santa Cruz Biotechnology. Anti-NUBP1 (NBP1–92204) and NUBP2 (NBP1–84533) were from Novus Biologicals. Anti-FAM96B (ab166607), POLD1 (ab10362), ELP3 (ab190907), ERCC2 (ab54676), FASN (ab128870), MOCS3 (ab154107) and CIAPIN1 (ab57551) were from Abcam. Anti-V5 (V8137), HSPA9 (HPA000898), HSCB (HPA018447), tubulin (T9026) and β-actin (A2228) were from Sigma. Anti-MMS19 (16015–1-AP), POLD1 (15646–1-AP), CIAPIN1 (12638–1-AP), GLRX3 (11254–1-AP) and URM1 (15285–1-AP) were from Proteintech. Anti-PPAT (PA5–12333) was from Thermo Scientific. Anti-GLRX3 (H00010539-M01) was from Abnova. Anti-NFS1 and ISCU rabbit polyclonal sera were raised against synthetic peptide fragments, as previously reported (22–24).

Statistical analyses

Where applicable, data were expressed as the mean ± standard error of the mean (SEM). Pairwise comparisons between two groups were analyzed using the unpaired Student's *t*-test.

Densitometry of band intensities

Where applicable, quantification of band intensities was performed using ImageJ.

Supplementary Material

Supplementary Material is available at *HMG* online.

Acknowledgements

We thank our colleagues in the Rouault laboratory for insightful discussions, Dr Crooks D. R. for suggesting the idea of generating and expressing the dominant negative mutant of cytosolic ISCU, ISCU1^{D46A}, the Eunice Kennedy Shriver NICHD Intramural Research Program for support and Dr Ross Tomaino for the MS analyses.

Conflict of Interest statement. None declared.

Funding

Intramural Research Program of the *Eunice Kennedy Shriver* National Institute of Child Health and Human Development.

Authors' Contribution

K.S.K., N.M. and T.A.R. designed the study. K.S.K. and N.M. performed most experiments; A.S. helped with experiments and in cell culture work. N.M. and T.A.R. wrote the manuscript. K.S.K., N.M. and T.A.R. analyzed the data. T.A.R. supervised the study.

References

1. Rudolf, J., Makrantoni, V., Ingledew, W.J., Stark, M.J. and White, M.F. (2006) The DNA repair helicases XPD and FancJ have essential iron-sulfur domains. *Mol. Cell*, **23**, 801–808.
2. Klinge, S., Hirst, J., Maman, J.D., Krude, T. and Pellegrini, L. (2007) An iron-sulfur domain of the eukaryotic primase is essential for RNA primer synthesis. *Nat. Struct. Mol. Biol.*, **14**, 875–877.
3. Pokharel, S. and Campbell, J.L. (2012) Cross talk between the nuclease and helicase activities of Dna2: role of an essential iron-sulfur cluster domain. *Nucleic Acids Res.*, **40**, 7821–7830.
4. Netz, D.J., Stith, C.M., Stumpfig, M., Kopf, G., Vogel, D., Genau, H.M., Stodola, J.L., Lill, R., Burgers, P.M. and Pierik, A.J. (2012) Eukaryotic DNA polymerases require an iron-sulfur cluster for the formation of active complexes. *Nat. Chem. Biol.*, **8**, 125–132.
5. Fuss, J.O., Tsai, C.L., Ishida, J.P. and Tainer, J.A. (2015) Emerging critical roles of Fe-S clusters in DNA replication and repair. *Biochim. Biophys. Acta*, **1853**, 1253–1271.
6. O'Brien, E., Holt, M.E., Thompson, M.K., Salay, L.E., Ehlinger, A.C., Chazin, W.J. and Barton, J.K. (2017) The [4Fe4S] cluster of human DNA primase functions as a redox switch using DNA charge transport. *Science*, **355**, eaag1789.
7. Bartels, P.L., Zhou, A., Arnold, A.R., Nunez, N.N., Crespilho, F.N., David, S.S. and Barton, J.K. (2017) Electrochemistry of the [4Fe4S] cluster in base excision repair proteins: tuning the redox potential with DNA. *Langmuir*, **33**, 2523–2530.
8. Lill, R., Dutkiewicz, R., Freibert, S.A., Heidenreich, T., Mascarenhas, J., Netz, D.J., Paul, V.D., Pierik, A.J., Richter, N., Stumpfig, M. *et al.* (2015) The role of mitochondria and the CIA machinery in the maturation of cytosolic and nuclear iron-sulfur proteins. *Eur. J. Cell Biol.*, **94**, 280–291.
9. Maio, N. and Rouault, T.A. (2015) Iron-sulfur cluster biogenesis in mammalian cells: new insights into the molecular mechanisms of cluster delivery. *Biochim. Biophys. Acta*, **1853**, 1493–1512.
10. Rouault, T.A. and Maio, N. (2017) Biogenesis and functions of mammalian iron-sulfur proteins in the regulation of iron homeostasis and pivotal metabolic pathways. *J. Biol. Chem.*, **292**, 12744–12753.
11. Cory, S.A., Van Vranken, J.G., Brignole, E.J., Patra, S., Winge, D.R., Drennan, C.L., Rutter, J. and Barondeau, D.P. (2017) Structure of human Fe-S assembly subcomplex reveals unexpected cysteine desulfurase architecture and acyl-ACP-ISD11 interactions. *Proc. Natl. Acad. Sci. U S A*, **114**, E5325–E5334.
12. Ciesielski, S.J., Schilke, B.A., Osipiuk, J., Bigelow, L., Mulligan, R., Majewska, J., Joachimiak, A., Marszalek, J., Craig, E.A. and Dutkiewicz, R. (2012) Interaction of J-protein co-chaperone Jac1 with Fe-S scaffold Isu is indispensable in vivo and conserved in evolution. *J. Mol. Biol.*, **417**, 1–12.
13. Vickery, L.E. and Cupp-Vickery, J.R. (2007) Molecular chaperones HscA/Ssq1 and HscB/Jac1 and their roles in iron-sulfur protein maturation. *Crit. Rev. Biochem. Mol. Biol.*, **42**, 95–111.
14. Uhrigshardt, H., Singh, A., Kovtunovych, G., Ghosh, M. and Rouault, T.A. (2010) Characterization of the human HSC20, an unusual DnaJ type III protein, involved in iron-sulfur cluster biogenesis. *Hum. Mol. Genet.*, **19**, 3816–3834.
15. Maio, N., Singh, A., Uhrigshardt, H., Saxena, N., Tong, W.H. and Rouault, T.A. (2014) Cochaperone binding to LYR motifs confers specificity of iron sulfur cluster delivery. *Cell Metab.*, **19**, 445–457.
16. Kispal, G., Csere, P., Prohl, C. and Lill, R. (1999) The mitochondrial proteins Atm1p and Nfs1p are essential for biogenesis of cytosolic Fe/S proteins. *EMBO J.*, **18**, 3981–3989.
17. Nakai, Y., Nakai, M., Hayashi, H. and Kagamiyama, H. (2001) Nuclear localization of yeast Nfs1p is required for cell survival. *J. Biol. Chem.*, **276**, 8314–8320.
18. Gerber, J., Neumann, K., Prohl, C., Muhlenhoff, U. and Lill, R. (2004) The yeast scaffold proteins Isu1p and Isu2p are required inside mitochondria for maturation of cytosolic Fe/S proteins. *Mol. Cell. Biol.*, **24**, 4848–4857.
19. Schilke, B., Voisine, C., Beinert, H. and Craig, E. (1999) Evidence for a conserved system for iron metabolism in the mitochondria of Saccharomyces cerevisiae. *Proc. Natl. Acad. Sci. U S A*, **96**, 10206–10211.
20. Land, T. and Rouault, T.A. (1998) Targeting of a human iron-sulfur cluster assembly enzyme, nifs, to different subcellular compartments is regulated through alternative AUG utilization. *Mol. Cell*, **2**, 807–815.
21. Shi, Y., Ghosh, M.C., Tong, W.H. and Rouault, T.A. (2009) Human ISD11 is essential for both iron-sulfur cluster assembly and maintenance of normal cellular iron homeostasis. *Hum. Mol. Genet.*, **18**, 3014–3025.
22. Li, K., Tong, W.H., Hughes, R.M. and Rouault, T.A. (2006) Roles of the mammalian cytosolic cysteine desulfurase, ISCS, and scaffold protein, ISCU, in iron-sulfur cluster assembly. *J. Biol. Chem.*, **281**, 12344–12351.
23. Tong, W.H. and Rouault, T.A. (2006) Functions of mitochondrial ISCU and cytosolic ISCU in mammalian iron-sulfur cluster biogenesis and iron homeostasis. *Cell Metab.*, **3**, 199–210.
24. Tong, W.H., Jameson, G.N., Huynh, B.H. and Rouault, T.A. (2003) Subcellular compartmentalization of human Nfu, an iron-sulfur cluster scaffold protein, and its ability to assemble a [4Fe-4S] cluster. *Proc. Natl. Acad. Sci. U S A*, **100**, 9762–9767.
25. Thul, P.J., Akesson, L., Wiking, M., Mahdessian, D., Geladaki, A., Ait Blal, H., Alm, T., Asplund, A., Bjork, L., Breckels, L.M. *et al.* (2017) A subcellular map of the human proteome. *Science*, **356**, eaal3321.
26. Marelja, Z., Mullick Chowdhury, M., Dosche, C., Hille, C., Baumann, O., Löhmannsröben, H.-G., Leimkühler, S. and Missirlis, F. (2013) The L-cysteine desulfurase NFS1 is localized in the cytosol where it provides the sulfur for molybdenum cofactor biosynthesis in humans. *PLoS One*, **8**, e60869.
27. Frasdorf, B., Radon, C. and Leimkuhler, S. (2014) Characterization and interaction studies of two isoforms of the dual localized 3-mercaptopyruvate sulfurtransferase TUM1 from humans. *J. Biol. Chem.*, **289**, 34543–34556.
28. Nakai, Y., Umeda, N., Suzuki, T., Nakai, M., Hayashi, H., Watanabe, K. and Kagamiyama, H. (2004) Yeast Nfs1p is

involved in thio-modification of both mitochondrial and cytoplasmic tRNAs. *J. Biol. Chem.*, **279**, 12363–12368.
29. Muhlenhoff, U., Balk, J., Richhardt, N., Kaiser, J.T., Sipos, K., Kispal, G. and Lill, R. (2004) Functional characterization of the eukaryotic cysteine desulfurase Nfs1p from Saccharomyces cerevisiae. *J. Biol. Chem.*, **279**, 36906–36915.
30. Tong, W.H. and Rouault, T. (2000) Distinct iron-sulfur cluster assembly complexes exist in the cytosol and mitochondria of human cells. *EMBO J.*, **19**, 5692–5700.
31. Maio, N., Kim, K.S., Singh, A. and Rouault, T.A. (2017) A single adaptable cochaperone-scaffold complex delivers nascent iron-sulfur clusters to mammalian respiratory chain complexes I-III. *Cell Metab.*, **25**, 945–953.
32. Kim, R., Saxena, S., Gordon, D.M., Pain, D. and Dancis, A. (2001) J-domain protein, Jac1p, of yeast mitochondria required for iron homeostasis and activity of Fe-S cluster proteins. *J. Biol. Chem.*, **276**, 17524–17532.
33. Voisine, C., Cheng, Y.C., Ohlson, M., Schilke, B., Hoff, K., Beinert, H., Marszalek, J. and Craig, E.A. (2001) Jac1, a mitochondrial J-type chaperone, is involved in the biogenesis of Fe/S clusters in Saccharomyces cerevisiae. *Proc. Natl. Acad. Sci. U S A*, **98**, 1483–1488.
34. Uhrigshardt, H., Rouault, T.A. and Missirlis, F. (2013) Insertion mutants in Drosophila melanogaster Hsc20 halt larval growth and lead to reduced iron-sulfur cluster enzyme activities and impaired iron homeostasis. *J. Biol. Inorg. Chem.*, **18**, 441–449.
35. Lill, R. (2015) Mechanisms of intracellular compartmentalization and disease. *Eur. J. Cell Biol.*, **94**, 277–279.
36. Xu, X.M., Lin, H., Latijnhouwers, M., Møller, S.G. and Newbigin, E. (2009) Dual localized AtHscB involved in iron sulfur protein biogenesis in Arabidopsis. *PLoS One*, **4**, e7662.
37. Gari, K., Leon Ortiz, A.M., Borel, V., Flynn, H., Skehel, J.M. and Boulton, S.J. (2012) MMS19 links cytoplasmic iron-sulfur cluster assembly to DNA metabolism. *Science*, **337**, 243–245.
38. Stehling, O., Vashisht, A.A., Mascarenhas, J., Jonsson, Z.O., Sharma, T., Netz, D.J., Pierik, A.J., Wohlschlegel, J.A. and Lill, R. (2012) MMS19 assembles iron-sulfur proteins required for DNA metabolism and genomic integrity. *Science*, **337**, 195–199.
39. Tubbs, A. and Nussenzweig, A. (2017) Endogenous DNA damage as a source of genomic instability in cancer. *Cell*, **168**, 644–656.
40. Barnes, R. and Eckert, K. (2017) Maintenance of genome integrity: how mammalian cells orchestrate genome duplication by coordinating replicative and specialized DNA polymerases. *Genes (Basel)*, **8**, 19.
41. Palovcak, A., Liu, W., Yuan, F. and Zhang, Y. (2017) Maintenance of genome stability by Fanconi anemia proteins. *Cell Biosci.*, **7**, 8.
42. Frey, A.G., Palenchar, D.J., Wildemann, J.D. and Philpott, C.C. (2016) A glutaredoxin-BolA complex serves as an iron-sulfur cluster chaperone for the cytosolic cluster assembly machinery. *J. Biol. Chem.*, **291**, 22344–22356.
43. Zhang, Y., Lyver, E.R., Nakamaru-Ogiso, E., Yoon, H., Amutha, B., Lee, D.-W., Bi, E., Ohnishi, T., Daldal, F., Pain, D. and Dancis, A. (2008) Dre2, a conserved eukaryotic Fe/S cluster protein, functions in cytosolic Fe/S protein biogenesis. *Mol. Cell. Biol.*, **28**, 5569–5582.
44. Bitto, E., Bingman, C.A., Bittova, L., Kondrashov, D.A., Bannen, R.M., Fox, B.G., Markley, J.L. and Phillips, G.N. Jr. (2008) Structure of human J-type co-chaperone HscB reveals a tetracysteine metal-binding domain. *J. Biol. Chem.*, **283**, 30184–30192.
45. McCarty, A.S., Kleiger, G., Eisenberg, D. and Smale, S.T. (2003) Selective dimerization of a C2H2 zinc finger subfamily. *Mol. Cell*, **11**, 459–470.
46. Liu, H., Liu, J.Y., Wu, X. and Zhang, J.T. (2010) Biochemistry, molecular biology, and pharmacology of fatty acid synthase, an emerging therapeutic target and diagnosis/prognosis marker. *Int. J. Biochem. Mol. Biol.*, **1**, 69–89.
47. Cai, K., Frederick, R.O., Tonelli, M. and Markley, J.L. (2017) Mitochondrial cysteine desulfurase and ISD11 coexpressed in *Escherichia coli* yield complex containing Acyl carrier protein. *ACS Chem. Biol.*, **12**, 918–921.
48. Van Vranken, J.G., Jeong, M.Y., Wei, P., Chen, Y.C., Gygi, S.P., Winge, D.R. and Rutter, J. (2016) The mitochondrial acyl carrier protein (ACP) coordinates mitochondrial fatty acid synthesis with iron sulfur cluster biogenesis. *Elife*, **5**.
49. Boniecki, M.T., Freibert, S.A., Muhlenhoff, U., Lill, R. and Cygler, M. (2017) Structure and functional dynamics of the mitochondrial Fe/S cluster synthesis complex. *Nat. Commun.*, **8**, 1287.
50. Marelja, Z., Stocklein, W., Nimtz, M. and Leimkuhler, S. (2008) A novel role for human Nfs1 in the cytoplasm: Nfs1 acts as a sulfur donor for MOCS3, a protein involved in molybdenum cofactor biosynthesis. *J. Biol. Chem.*, **283**, 25178–25185.
51. Marinoni, E.N., de Oliveira, J.S., Nicolet, Y., Raulfs, E.C., Amara, P., Dean, D.R. and Fontecilla-Camps, J.C. (2012) (IscS-IscU)2 complex structures provide insights into Fe2S2 biogenesis and transfer. *Angew. Chem. Int. Ed. Engl.*, **51**, 5439–5442.
52. Raulfs, E.C., O'Carroll, I.P., Dos Santos, P.C., Unciuleac, M.C. and Dean, D.R. (2008) In vivo iron-sulfur cluster formation. *Proc. Natl. Acad. Sci. U S A*, **105**, 8591–8596.
53. Unciuleac, M.C., Chandramouli, K., Naik, S., Mayer, S., Huynh, B.H., Johnson, M.K. and Dean, D.R. (2007) In vitro activation of apo-aconitase using a [4Fe-4S] cluster-loaded form of the IscU [Fe-S] cluster scaffolding protein. *Biochemistry*, **46**, 6812–6821.
54. Maio, N., Ghezzi, D., Verrigni, D., Rizza, T., Bertini, E., Martinelli, D., Zeviani, M., Singh, A., Carrozzo, R. and Rouault, T.A. (2016) Disease-causing SDHAF1 mutations impair transfer of Fe-S clusters to SDHB. *Cell Metab.*, **23**, 292–302.
55. Odermatt, D.C. and Gari, K. (2017) The CIA targeting complex is highly regulated and provides two distinct binding sites for client iron-sulfur proteins. *Cell Rep.*, **18**, 1434–1443.
56. Majewska, J., Ciesielski, S.J., Schilke, B., Kominek, J., Blenska, A., Delewski, W., Song, J.Y., Marszalek, J., Craig, E.A. and Dutkiewicz, R. (2013) Binding of the chaperone Jac1 protein and cysteine desulfurase Nfs1 to the iron-sulfur cluster scaffold Isu protein is mutually exclusive. *J. Biol. Chem.*, **288**, 29134–29142.
57. Netz, D.J., Pierik, A.J., Stumpfig, M., Muhlenhoff, U. and Lill, R. (2007) The Cfd1-Nbp35 complex acts as a scaffold for iron-sulfur protein assembly in the yeast cytosol. *Nat. Chem. Biol.*, **3**, 278–286.
58. Stehling, O., Netz, D.J., Niggemeyer, B., Rosser, R., Eisenstein, R.S., Puccio, H., Pierik, A.J. and Lill, R. (2008) Human Nbp35 is essential for both cytosolic iron-sulfur protein assembly and iron homeostasis. *Mol. Cell. Biol.*, **28**, 5517–5528.
59. Stehling, O., Mascarenhas, J., Vashisht, A.A., Sheftel, A.D., Niggemeyer, B., Rosser, R., Pierik, A.J., Wohlschlegel, J.A. and Lill, R. (2013) Human CIA2A-FAM96A and CIA2B-FAM96B integrate iron homeostasis and maturation of different

subsets of cytosolic-nuclear iron-sulfur proteins. *Cell Metab.*, **18**, 187–198.
60. Paul, V.D., Muhlenhoff, U., Stumpfig, M., Seebacher, J., Kugler, K.G., Renicke, C., Taxis, C., Gavin, A.C., Pierik, A.J. and Lill, R. (2015) The deca-GX3 proteins Yae1-Lto1 function as adaptors recruiting the ABC protein Rli1 for iron-sulfur cluster insertion. *Elife*, **4**, e08231.
61. Johnson, N.B., Deck, K.M., Nizzi, C.P. and Eisenstein, R.S. (2017) A synergistic role of IRP1 and FBXL5 proteins in coordinating iron metabolism during cell proliferation. *J. Biol. Chem.*, **292**, 15976–15989.
62. Veatch, J.R., McMurray, M.A., Nelson, Z.W. and Gottschling, D.E. (2009) Mitochondrial dysfunction leads to nuclear genome instability via an iron-sulfur cluster defect. *Cell*, **137**, 1247–1258.
63. Bedekovics, T., Li, H., Gajdos, G.B. and Isaya, G. (2011) Leucine biosynthesis regulates cytoplasmic iron-sulfur enzyme biogenesis in an Atm1p-independent manner. *J. Biol. Chem.*, **286**, 40878–40888.
64. Pondarre, C., Antiochos, B.B., Campagna, D.R., Clarke, S.L., Greer, E.L., Deck, K.M., McDonald, A., Han, A.P., Medlock, A. and Kutok, J.L. (2006) The mitochondrial ATP-binding cassette transporter Abcb7 is essential in mice and participates in cytosolic iron-sulfur cluster biogenesis. *Hum. Mol. Genet.*, **15**, 953–964.
65. Pondarre, C., Campagna, D.R., Antiochos, B., Sikorski, L., Mulhern, H. and Fleming, M.D. (2007) Abcb7, the gene responsible for X-linked sideroblastic anemia with ataxia, is essential for hematopoiesis. *Blood*, **109**, 3567–3569.
66. Cavadini, P., Biasiotto, G., Poli, M., Levi, S., Verardi, R., Zanella, I., Derosas, M., Ingrassia, R., Corrado, M. and Arosio, P. (2007) RNA silencing of the mitochondrial ABCB7 transporter in HeLa cells causes an iron-deficient phenotype with mitochondrial iron overload. *Blood*, **109**, 3552–3559.
67. Miao, R., Kim, H., Koppolu, U.M., Ellis, E.A., Scott, R.A. and Lindahl, P.A. (2009) Biophysical characterization of the iron in mitochondria from Atm1p-depleted Saccharomyces cerevisiae. *Biochemistry*, **48**, 9556–9568.
68. Desler, C., Lykke, A. and Rasmussen, L.J. (2010) The effect of mitochondrial dysfunction on cytosolic nucleotide metabolism. *J. Nucleic Acids*, **2010**, 1.
69. Gebauer, F. and Hentze, M.W. (2004) Molecular mechanisms of translational control. *Nat. Rev. Mol. Cell Biol.*, **5**, 827–835.
70. Jackson, R.J., Hellen, C.U. and Pestova, T.V. (2010) The mechanism of eukaryotic translation initiation and principles of its regulation. *Nat. Rev. Mol. Cell Biol.*, **11**, 113–127.
71. White, M.F. and Dillingham, M.S. (2012) Iron-sulphur clusters in nucleic acid processing enzymes. *Curr. Opin. Struct. Biol.*, **22**, 94–100.
72. Paul, A., Drecourt, A., Petit, F., Deguine, D.D., Vasnier, C., Oufadem, M., Masson, C., Bonnet, C., Masmoudi, S., Mosnier, I. *et al.* (2017) FDXR mutations cause sensorial neuropathies and expand the spectrum of mitochondrial Fe-S-synthesis diseases. *Am. J. Hum. Genet.*, **101**, 630–637.
73. Peng, Y., Shinde, D.N., Valencia, A.C., Mo, J.S., Rosenfeld, J., Truitt Cho, M., Chamberlin, A., Li, Z., Liu, J., Gui, B. *et al.* (2017) Biallelic mutations in the ferredoxin reductase gene cause novel mitochondriopathy with optic atrophy. *Hum. Mol. Genet.*, **26**, 4937–4950.
74. Eng, J.K., McCormack, A.L. and Yates, J.R. (1994) An approach to correlate tandem mass spectral data of peptides with amino acid sequences in a protein database. *J. Am. Soc. Mass Spectrom.*, **5**, 976–989.